



NRL/MR/6110--06-9002

Methane Hydrate Exploration, Atwater Valley, Texas-Louisiana Shelf: Geophysical and Geochemical Profiles

RICHARD B. COFFIN

*Chemical Dynamics and Diagnostics Branch
Chemistry Division*

JOAN GARDNER

*Marine Physics Branch
Marine Geosciences Division*

JOHN POHLMAN

*VIMS
Gloucester Point, VA*

ROSS DOWNER

*Milbar-Hydrotest, Inc.
Shreveport, LA*

WARREN WOOD

*Seafloor Sciences Branch
Marine Geosciences Division*

December 27, 2006

Approved for public release; distribution is unlimited.

Cruise Report

RV Gyre, May 10-20, 2004

Methane Hydrate Exploration, Atwater Valley, Texas-Louisiana Shelf: Geophysical and Geochemical Profiles

Richard Coffin, NRL, Code 6114

Joan Gardner, NRL, Code 7420

John Pohlman, VIMS

Ross Downer, Milbar Hydrotest, Inc.

Warren Wood, NRL, 7432

POC: Richard Coffin, NRL Code 6114, rcoffin@ccs.nrl.navy.mil, 202-767-0065

ii. **DISCLAIMER**

This report was prepared as an account of work sponsored by an agency of the United States Government. Neither the United States Government nor any agency thereof, nor any of their employees, makes any warranty, express or implied, or assumes any legal liability of responsibility for the accuracy, completeness, or usefulness of any information, apparatus product, or process disclosed, or represents that its use would not infringe privately owned rights. Reference herein to any specific commercial product, process, or service by trade name, trademark, manufacturer, or otherwise does not necessarily constitute or imply its endorsement, recommendation, or favoring by the United States Government or any agency thereof. The views and opinions of authors expressed herein do not necessarily state or reflect those of the United States Government or any agency thereof.

iii. TABLE OF CONTENTS

page number

i.	Title Page	1
ii.	Disclaimer.....	2
iii.	Table of Contents.....	3
iv.	List of Figures.....	4
v.	List of Tables.....	5
vi.	List of Appendices.....	5
vii.	Abstract.....	6
I.	Introduction.....	7
II.	General Information	8
III.	Methods.....	13
IV.	Preliminary Results.....	17
V.	Summary.....	30
VI.	Future Goals.....	31
VII.	Acknowledgements.....	31
VIII.	Literature Cited.....	32

iv. LIST OF FIGURES

page number

Figure 1: Atwater Valley location along the Texas-Louisiana Shelf in the Gulf of Mexico.....	9
Figure 2: Piston core and heatflow sample positions on Atwater Valley.....	10
Figure 3: NRL piston core and heatflow transect sites presented over a 3.5 kHz transect through the sample region.....	10
Figure 4: A portion of USGS multichannel seismic line AV65 over Mound F.....	11
Figure 5: A portion of USGS multichannel seismic line AV65 over Mound D.....	11
Figure 6: Piston core CH ₄ and SO ₄ ⁻² profiles of stations located between the USGS seismic survey observation of mound D and mound F.....	18
Figure 7: Piston core CH ₄ and SO ₄ ⁻² profiles of stations located on mound F that was identified on a USGS seismic survey.....	18
Figure 8: Piston core CH ₄ and SO ₄ ⁻² profiles of stations located to the north (core 6) and south (core 9) of mound F.....	19
Figure 9: Example piston core pore water data applied to predict deep sediment methane.....	20
Figure 10: DIC concentration and δ ¹³ C of DIC for Core 1 located in the center of the transect through Atwater Valley site between mound D and mound F.....	20
Figure 11: DIC concentrations and δ ¹³ C of DIC for Core 7 and Core 2 present the range in profiles taken during the Atwater Valley survey.....	21
Figure 12: Chloride profiles for piston core pore water samples.....	22
Figure 13: Comparison of pore water methane and chloride concentrations from cores on top of, on the edge and away from mound F.....	22
Figure 14: Pore water sulfate concentration profiles plotted relative to centimeters below the sea floor (cmbsf) for JIP sites along the Atwater Valley transect between mounds D and F.....	24
Figure 15: Pore water methane concentration profiles plotted relative to centimeters below the sea floor (cmbsf) for JIP sites along the Atwater Valley transect between mounds D and F.....	25

iv. LIST OF FIGURES (continued) page number

Figure 16: Pore water DIC concentration profiles plotted relative to centimeters below the sea floor (cmbsf) for JIP sites along the Atwater Valley transect between mounds D and 25

Figure 17: Pore water dissolved inorganic carbon concentration profiles plotted relative to centimeters below the sea floor (cmbsf) for JIP sites along the Atwater Valley transect between mounds D and F..... 26

Figure 18: Pore water chloride concentration profiles plotted relative to centimeters below the sea floor (cmbsf) for JIP sites along the Atwater Valley transect between mounds D and F 27

Figure 19: Temperature vs. depth plots for stations along transect over Mound F.. 28

Figure 20: Temperature vs. depth plots for stations along transect over Mound D.. 29

Figure 21. Thermal profiles for all thermistors along the entire transect..... 29

Figure 22. Heat flow profile for all stations along the transect..... 30

v. LIST OF TABLES

Table 1: Participating research scientists..... 8

Table 2: Locations, water depths, and penetration lengths of piston core and thermal probe sites. CMP number refers to USGS seismic line AV65 acquired in April 2003. JIP sites 1-5 are planned sites for deep drilling..... 12

Table 3: Core gas methane $\delta^{13}\text{C}$ data. Additional information includes vertical location of the gas pocket in the core, gas retention time (Rt) in the GC run and the area for the mass 44 peak. Standard deviations were calculated for samples from 180 cm in core 3 and 567 cm in core 23

vi. LIST OF APPENDICIES

Appendix 1: Pore Water Data..... 33

vii. ABSTRACT

From May 14 - 20, 2004 piston core and heat flow measurements were collected across two mound structures, mound D and mound F, in an area designated as Atwater Valley, a shallow trough on the continental slope south of the Mississippi Delta. Atwater Valley lies at 1,200 to 1,500 meters water depth. Several small mound structures occur in the valley, rising less than 50 meters above the surrounding seafloor. Coring plans were designed to support Chevron-Texaco JIP drilling completed during 2005. The USGS collected several multichannel seismic lines in this area in 2003. During 4 days on site we acquired 15 piston cores and 23 thermal profiles on a transect from mound F to mound D. A previous USGS seismic line (AV65) and a 3.5 kHz echosounder profile collected during the cruise were used to guide operations. All cores had good penetration, (shortest was 255 cm, longest 842 cm), and no carbonate pavement or hydrate mounds were encountered. The cores were immediately sectioned and sampled for chemical analysis. No detailed sedimentological examinations were made. All attempts at thermal probing resulted in sufficient penetration, except for one instance where the instrument laid horizontal on the seafloor.

The sulfate-methane interface (SMI) estimated from pore water sulfate profiles indicated a range in the vertical flux of methane. Sulfate and methane pore water profiles from piston cores on mound F indicated the greatest vertical methane flux in this study region. Sulfate was depleted in surface core samples and methane concentrations were elevated suggesting a flow of methane into the water column. Overall the SMI across the transect ranged from 45 to 410 cm. Stable carbon isotope ratios and speciation of gases sampled from the piston cores indicated a microbial source of methane. Chloride data from piston cores did not indicate hydrates were sampled and dissociated during transport from the sediment and deck processing. However, high chloride concentrations were measured on mound F. It is expected that the chloride originated from deep salt diapirs. DIC concentrations and stable carbon isotope analysis confirmed anaerobic methane oxidation in the pore water profiles. Mound F sites showed shallower DIC concentration peaks and more ^{13}C depletion in the DIC. These data are consistent with increased vertical methane flux in this region. Data were also sorted according to the Chevron-Texaco JIP planning for deep well drilling. Chevron-Texaco sites JIP-1 and JIP-5 are located on mound F. Methane, sulfate, chloride, DIC and DIC $\delta^{13}\text{C}$ all indicate this region is the most active in vertical methane flow. Sites JIP-2 (between mounds D and F), JIP-3 (between mounds D and F) and JIP-4 (mound D) were found to have deeper SMI profiles.

Heatflow probing was conducted at each of the piston coring sites; additional sites, relative to the piston coring, were included for more resolution. The data show clear anomalies in sediment temperature and heat flow associated with the mounds. Measurements collected on the top of mound F show elevated sediment temperatures, and heat flow values of around 160 mW/m^2 . Sediment temperatures decrease away from the summit of the mound, and heat flow values drop to a background level of 40 to 50 mW/m^2 . Sediment temperatures at the summit of Mound D are similar to what was observed at Mound F, and heat flow values are slightly lower at around 132 mW/m^2 , partly as a result of the slightly higher bottom water temperature and thus reduced thermal gradient. Away from the summit of Mound D the thermal gradient decreases and heat flow values drop to around 50 mW/m^2 .

I. INTRODUCTION

A tremendous quantity of methane hydrate, clathrate, is embedded in the sea floor along most continental margins of the world, and in permafrost at high latitudes. Distribution of organic carbon in the earth's crust in methane hydrates in oceans and the permafrost regions is estimated to be more than twice that contained in recoverable and non-recoverable fossil fuel (including coal, oil and natural gas). If extracted, the quantity of methane trapped in ocean sediments represents a large potential energy resource. The U.S. Geological Survey estimates the resource potential in the United States to be about 200,000 trillion cubic feet. The current annual consumption of natural gas is about 22 trillion cubic feet. Based on these estimates, at about 1% recovery the deposit has the potential to fill the natural gas needs of the nation, at the present rate of consumption, for the next 100 years. Additionally, for direct fuel combustion methane not only provides high energy density per weight, but relatively low CO₂ emissions. While a great deal of research is underway to understand the nature of hydrate deposits in the oceans and the permafrost regions, the safe and economic extraction of methane from hydrates is not close at hand. Besides the potential as an energy source, methane hydrates are also important to global climate, coastal slope stability, ocean carbon cycling and global economy. The U. S. Geological Survey and the Naval Research Laboratory are engaged in field and laboratory work designed to evaluate the hydrate resource in the Gulf of Mexico.

This project was designed to study methane hydrate distribution in the Atwater Valley, on the Texas-Louisiana Shelf, in the Gulf of Mexico. The hydrate survey was conducted with integration of seismic profiles, heatflow probing, and geochemical analysis of piston cores. The principal goals of this project were to: 1) test integration of geophysical and geochemical parameters to evaluate methane hydrate distribution; 2) develop of a more thorough data base for understanding methane hydrate distribution, 3) provide a field evaluation to support planning of the Chevron-Texaco JIP deep drilling in this region, and 4) compare the Chevron-Texaco deep drilling with the geochemical/geophysical prediction of deep sediment hydrate distribution. Data obtained from this survey contributes to the NRL database being developed from research off the US, Canadian, Chilean and Japanese coasts.

Piston cores were analyzed for hydrate presence, pore water chemistry and the source of the methane in the hydrates. Parameters include sulfate, chloride and stable carbon isotope analysis of DIC in pore waters and methane from gas pockets in the sediment core liner. Seismic data were used to constrain interpretation of the geochemical data. Sulfate and methane profiles were used to assess the vertical flux of methane. Stable carbon isotope analyses were used to determine whether the source of methane is thermogenic or microbial in origin.

In past research along the Texas-Louisiana Shelf hydrate gases have been found to be of thermogenic origin. NRL analysis of gas composition and stable carbon isotope ratios of 19 cores from Keathley Canyon during the August 2003 cruise found that the methane was through microbial production. There was no evidence for any significant (>0.1%) thermogenic gas input. The geochemical survey of Atwater Valley will provide an interesting comparison to similar data obtained from Keathley Canyon and other locations.

II. GENERAL INFORMATION

1. Environmental Effects

The heat flow probe and piston coring devices are each approximately 10 cm in diameter and penetrate the sea floor for up to 8 m and can cause some disturbance to the sea floor during penetration and removal. The piston coring also recovers samples of the shallow seafloor that are used for chemical analysis. There were 23 heat flow stations and about 15 piston cores through the two focus sites, mounds D and F. This equipment is standard equipment used by the academic and research community extensively in most of the oceans of the world. The measurements are routine, and disturbance of the sea floor is expected to be minimal. MMS verified that there were no man-made structures in either area that might be damaged by the use of these devices. The seismic data was acquired prior to coring and thermometry and preliminary imaging to provide an outline for locations of hard ground, which were avoided not only to protect chemosynthetic communities but also to prevent damage to the equipment.

2. Participants

Table 1: Participating research scientists

Scientist	Affiliation	Responsibility	Phone Number	Email
Dr. Richard Coffin	NRL, Code 6114	Chief Scientist	202-767-0065	rcoffin@ccs.nrl.navy.mil
Dr. Joan Gardner	NRL, Code 7420	Heatflow	202-404-1094	gardner@qur.nrl.navy.mil
Ross Downer	Milbar Hydrotest Inc.	Piston Coring	318-227-8210	rdowner@milbarhydro-test.com
John Pohlman	VIMS	Onboard Lab	202-404-3365	johnp@ccs.nrl.navy.mil
Dr. Warren Wood	NRL, Code 7432	Geophysic input	228-688-5311	warren.wood@nrlssc.navy.mil
Dr. Richard Hagen	NRL, Code 7420	Heatflow	202-404-1125	rhagen@qur.nrl.navy.mil
Mike Olson	Milbar Hydrotest Inc.	Piston Coring	318-752-0623	molson42@hotmail.com
Daniel Bean	TAMU	Piston Coring	979-845-7536	dabean@ocean.tamu.edu
Brandon Yoza	HNEI	Lab Analysis	808-4	byoza@hawaii.edu
Kiara Smith	VIMS	Lab Analysis	757-874-7294	kiara@vims.edu
Mary Cathey	USC	Lab Analysis	864-958-1824	MCATHEY@sc.rr.com

3. Site Description

Heatflow measurements and piston cores were collected across two mound structures in an area designated as Atwater Valley, a shallow trough on the continental slope south of the Mississippi Delta, on the Texas-Louisiana Shelf, in the Gulf of Mexico (Figure 1). The UNOLS vessel *RV Gyre* was contracted to support this work. The work took place in about 1,300 m water depth through a 4 km transect at lat. 27.9356°N, lon. 89.2794°W (lease block Atwater Valley 14); coordinates are listed in Table 2. Total sampling included mounds D and F and a transect between the mounds. Previous USGS seismic lines AV65, AV97 and AV82 and a 3.5 kHz echosounder profile collected during the cruise were used to guide operations (Figure 2). These seismic data were used because the NRL DTAGS system planned for the cruise was not operational prior to departure from port. Data is available from a subsequent DTAGS operation on this site. Extensive piston coring and heatflow was conducted at mound F (Figures 3 & 4). Dense heat flow measurements and one piston core were obtained at mound D (Figures 3 & 5). All coring and heat flow measurements were conducted at the sites planned for deep drilling by

the Chevron-Texaco JIP. Data at these sites are compared in this report. Table 2 provides exact locations of the piston core and heat flow locations.

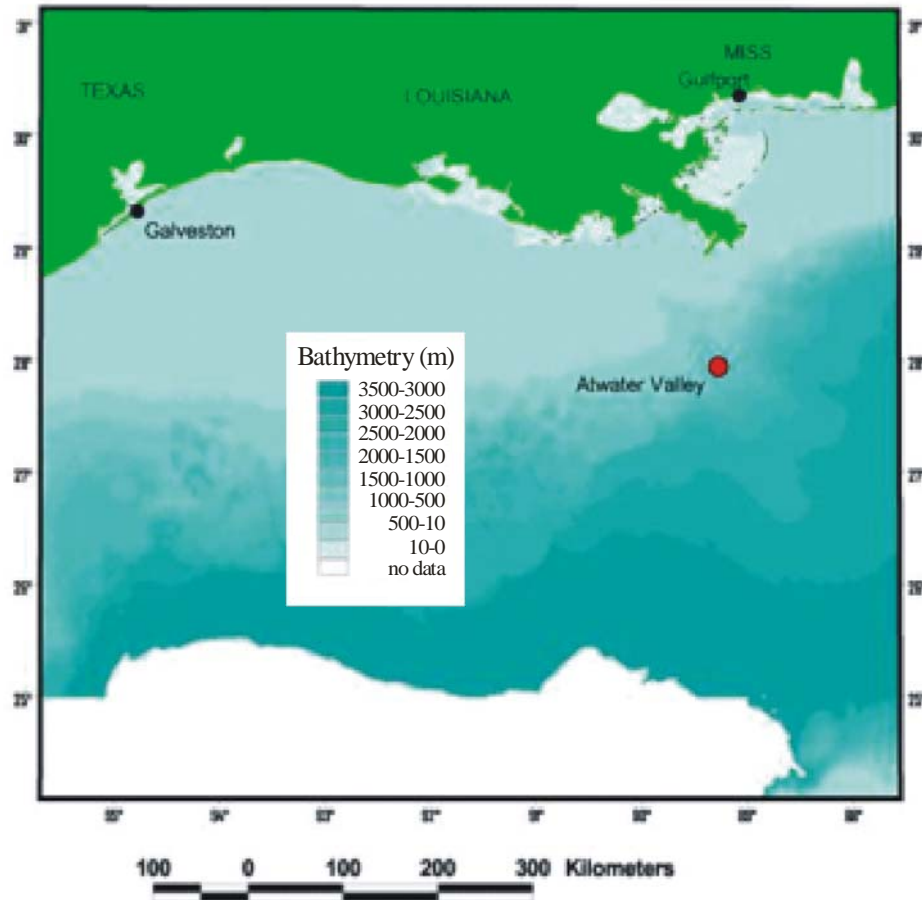


Figure 1: Atwater Valley location along the Texas-Louisiana Shelf in the Gulf of Mexico.

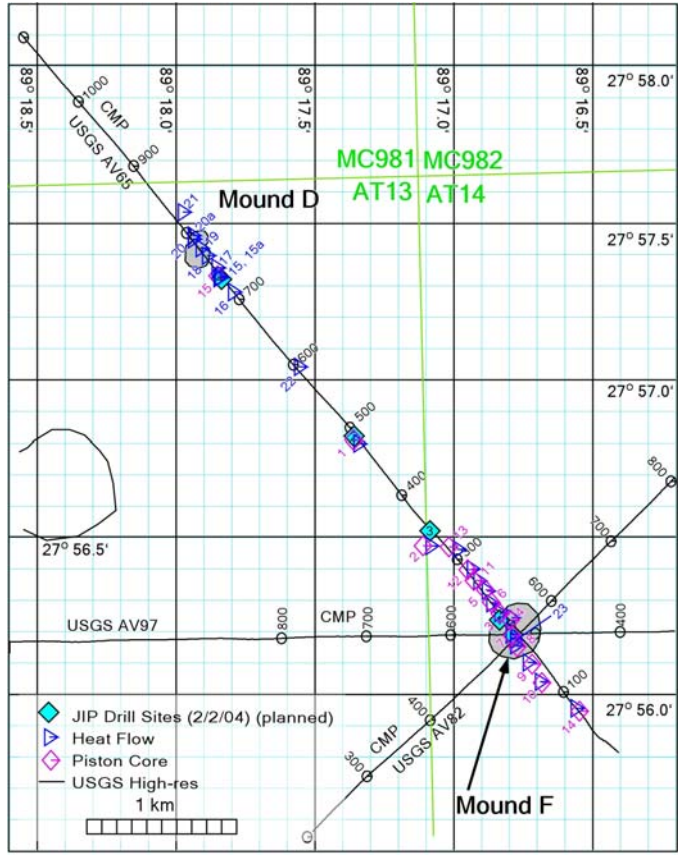


Figure 2: Piston core and heatflow sample positions on Atwater Valley.

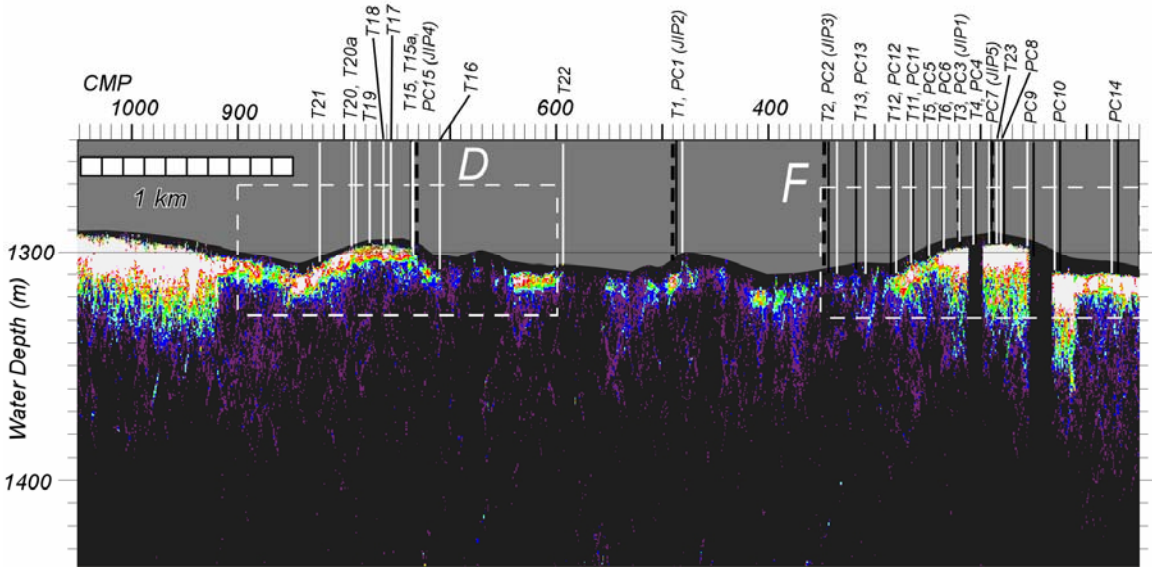


Figure 3: NRL piston core and heatflow transect sites presented over a 3.5 kHz transect through the sample region.

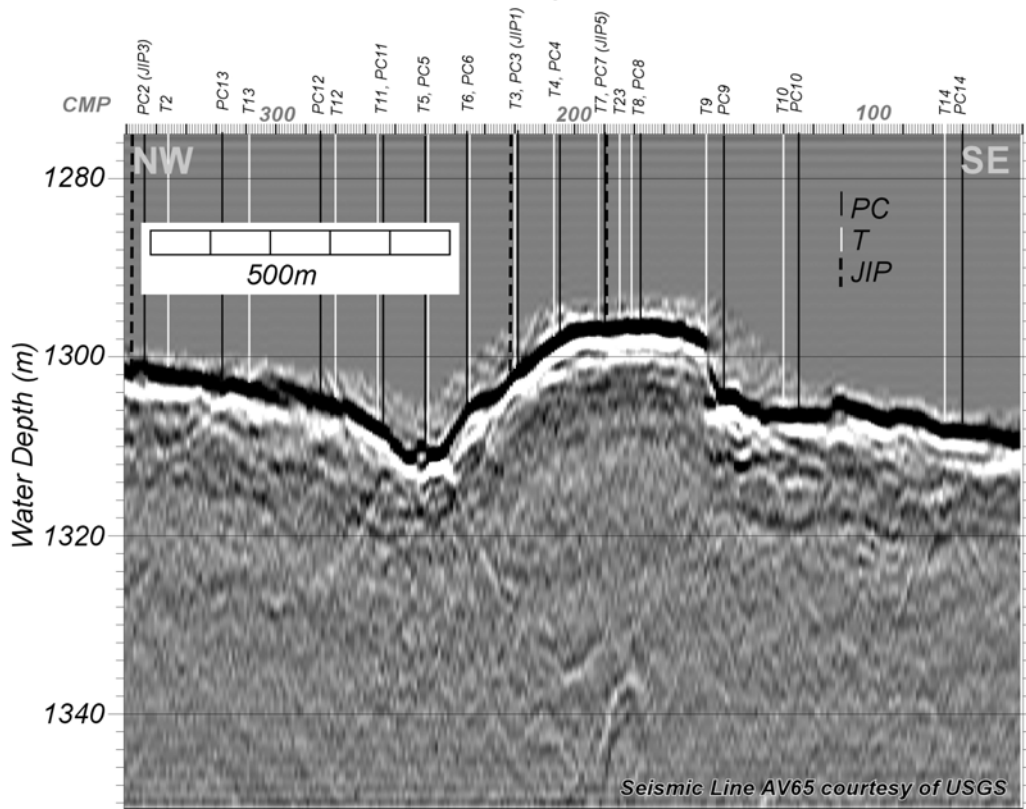


Figure 4. A portion of USGS multichannel seismic line AV65 over Mound F.

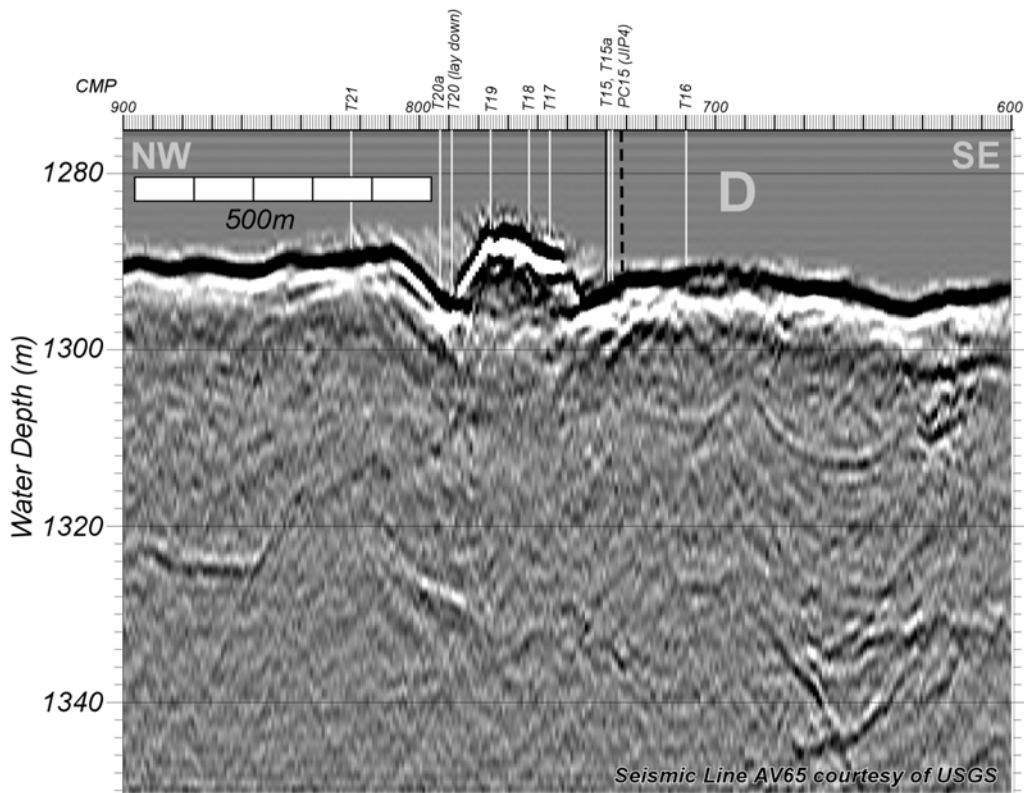


Figure 5. A portion of USGS multichannel seismic line AV65 over Mound D.

Table 2: Locations, water depths, and penetrations lengths of piston cores and thermal probe sites. CMP number refers to USGS seismic line AV65 acquired in April 2003. JIP sites 1-5 are planned sites for deep drilling. Chevron Texaco JIP focus site are listed under the sample column.

SAMPLE			LAT			LON	av65	LON	LAT	Water	Penet.
P Core	Deg	Min	Sec	Deg	Min	Sec	Cmp	dec deg	dec deg	Depth (m)	Length (m)
PC 1 (JIP2)	27	56	48.8	89	17	21.6	487	89.28933	27.94689	1292	2.70
PC 2 (JIP3)	27	56	28.644	89	17	6.629	344	89.28517	27.94129	1300	4.70
PC 3 (JIP1)	27	56	15.738	89	16	49.969	219	89.28055	27.93771	1301	3.70
PC 4	27	56	14.534	89	16	47.732	205	89.27993	27.93737	1298	8.38
PC 5	27	56	20.137	89	16	53.121	250	89.28142	27.93893	1310	3.46
PC 6	27	56	17.797	89	16	51.937	236	89.28109	27.93828	1305	5.12
PC 7 (JIP5)	27	56	11.508	89	16	47.356	190	89.27982	27.93653	1296	8.67
PC 8	27	56	9.514	89	16	46.247	178	89.27951	27.93598	1296	5.15
PC 9	27	56	6.189	89	16	43.101	150	89.27864	27.93505	1304	4.36
PC 10	27	56	2.437	89	16	40.942	125	89.27804	27.93401	1306	4.12
PC 11	27	56	21.998	89	16	55.766	264	89.28216	27.93944	1307	4.76
PC 12	27	56	24.084	89	16	56.983	285	89.2825	27.94002	1304	3.10
PC 13	27	56	28.378	89	17	0.924	17	89.28359	27.94122	1302	3.47
PC 14	27	55	56.881	89	16	32.79	70	89.27578	27.93247	1307	5.25
PC 15 (JIP4)	27	57	20.066	89	17	50.963	737	89.29749	27.95557	1292	3.40
HEAT											
T 1 (JIP2)	27	56	48.072	89	17	20.697	481	89.28908	27.94669	1292	3.00
T 2 (JIP3)	27	56	28.524	89	17	5.147	336	89.28476	27.94126	1301	3.00
T 3 (JIP1)	27	56	15.712	89	16	50.229	220	89.28062	27.9377	1302	3.00
T 4	27	56	14.781	89	16	47.582	207	89.27988	27.93744	1298	3.00
T 5	27	56	19.943	89	16	52.907	249	89.28136	27.93887	1310	3.00
T 6	27	56	17.546	89	16	51.969	235	89.2811	27.93821	1305	3.00
T 7 (JIP5)	27	56	11.595	89	16	47.774	192	89.27994	27.93655	1296	3.00
T 8	27	56	9.506	89	16	46.766	181	89.27966	27.93597	1296	3.00
T 9	27	56	6.242	89	16	44.124	156	89.27892	27.93507	1298	3.00
T 10	27	56	2.55	89	16	41.452	130	89.27818	27.93404	1306	3.00
T 11	27	56	21.889	89	16	54.746	266	89.28187	27.93941	1307	3.00
T 12	27	56	24.123	89	16	56.196	280	89.28228	27.94003	1305	3.00
T 13	27	56	27.853	89	16	59.271	309	89.28313	27.94107	1303	3.00
T 14	27	55	57.481	89	16	33.73	76	89.27604	27.93263	1307	3.00
T 15 (JIP4)	27	57	19.579	89	17	50.917	735	89.29748	27.95544	1293	3.00
T 15a (JIP4)	27	57	19.837	89	17	50.715	736	89.29742	27.95551	1293	3.00
T 16	27	57	16.91	89	17	47.841	710	89.29662	27.9547	1291	3.00
T 17	27	57	21.563	89	17	51.347	746	89.2976	27.95599	1288	3.00
T 18	27	57	23.865	89	17	53.473	763	89.29819	27.95663	1287	3.00
T 19	27	57	25.316	89	17	54.858	776	89.29857	27.95703	1287	3.00
T 20	27	57	27.048	89	17	56.504	789	89.29903	27.95751	1294	3.00
T 20a	27	57	27.711	89	17	56.595	793	89.29905	27.9577	1293	3.00
T 21	27	57	32.195	89	17	58.656	823	89.29963	27.95894	1289	3.00
T 22	27	57	2.656	89	17	33.478	595	89.29263	27.95074	1293	3.00
T 23	27	56	10.425	89	16	47.018	185	89.27973	27.93623	1296	3.00

4. Chronology

May 10-14 were spent at dock in Gulfport, MS mobilizing and waiting for DTAGS repair. By the afternoon of May 13, the decision was made to proceed with the piston coring and thermal probing portions of the cruise without DTAGS. In route a science meeting was held with Coffin, Gardner, Pohlman and Wood, at which the science plan was discussed and remaining on-site ship time allotted.

The RV Gyre arrived at the Atwater Valley site in the afternoon of May 14, the acoustic navigation transponder was deployed through the moon pool and one piston core was obtained before nightfall at JIP Site 2 (Figure 1). Piston cores 2-8 were acquired on May 15, and 9-15 were acquired on May 16. All deployments resulted in recovered samples, and all but PC1 and PC2 were acoustically navigated. The cable was re-rigged for the thermal probe at about 19:00, but because both winch operators were used all day in coring and were tired, thermal probe operations were postponed until morning.

The thermal probe was deployed at about 0900 May 17, three stations were acquired and the probe was brought up to download data, since no acoustic communication was available. Data were of good quality so the probe was redeployed this time for 5 stations, before being brought up to download data. Another deployment of 5 stations was acquired and the probe was brought on deck for charging overnight. These first 13 stations extensively sampled mound F.

On May 18 three more deployments resulted in 12 more stations (mostly over mound D) before science operations were ended at about 18:00, and preparations were made to transit to Galveston. All thermal probe sites were acoustically navigated. The return to Galveston required 37 hrs – the Gyre arrived in port about 08:30 May 20, 2004.

III. METHODS

1. Acoustic Navigation

On board the RV Gyre was a Sonardyne Fusion acoustic navigation system, consisting of a multi-element transceiver array (head) that was deployed through the moon pool via an hour long procedure requiring bolting the system to a bracket within the moon pool. Maximum speed with the transceiver deployed was 3.5 to 4 kts. A Sonardyne mini-transponder was the remote transponder, attached to the piston core cable 50 meters above the core head, and attached to the thermal probe cable 100 meters above the thermal probe weight stand. The vertical reference unit was fixed about 3 meters aft of the transponder, and all instruments were calibrated prior to the NRL personnel boarding the ship.

The acoustic tracking was largely successful but deeper than about 800 the position fix deteriorated significantly. This may be due to the transceiver being directed slightly aft, or possibly due to the relatively weaker signal from the mini-transponder as opposed to the full sized transponder for which the system was designed. The min-transponder was used because the only cable clamps available would not fit the full sized transponder. Deeper than about 800 the fixes appeared better if the remote transponder was greater than about 20 meters aft of the ship.

When good position fixes were obtained, we estimate they were accurate to within about 2-5 meters.

2. Piston Coring

Piston coring (PC) was conducted over the starboard side of the vessel. PC was conducted on a 24 hour basis. Because objectives include the recovery of methane hydrate, which melts very quickly when on deck, care was taken to quickly place the PC apparatus on deck, disassemble the core barrels, and inspect for samples before the samples melt. Because hydrogen sulfide fumes can be present in these areas all disassembly were outside, on deck, and all crew working with the PC were briefed on safety procedures. All PC stations planned were in about 1300 m of water, so at 60 meters per minute, transit time was about 22 minutes. Station locations (way points) for piston coring and heat flow were planed over Mounds D and F and through transects between the sites.

3. Pore Water

a. Press Loading and Squeezing - Whole round core sections were transported to the lab. Clean dry spatulas were used to scrape the surface sediment from the core and the surface material was discarded. Sediment from the interior of the core were scooped out and placed inside the body of the press. The press bodies were filled with sediment to maximum capacity in order to leave a minimum volume of air. A clean dental dam was place on the air inflow side of the press body to prevent free airflow through the core. The press bodies were capped and placed on the pore water press rack. Pore water was collected in a 60 ml syringe on the outflow line. Pressure through the line was constant with nitrogen gas. Sediment from the press was placed on a sheet of ashed Al foil and frozen.

b. Pore water Processing - Pore water fluid was extracted with a pressurized pore water sampler from 10-cm whole round core sections collected every 25-45 cm. A minimum of 7 mls pore water per sample was required. Using the side port on a three-port stopcock, 1 ml was removed from the 60 ml syringe with a 10 ml syringe for analysis of total sulfides. A 0.2 μm syringe filter and a 21 gauge needle was placed on the 60 ml syringe. The contents of the syringe were placed into a scintillation vial. Using a 1 ml fixed volume pipet, 2 mls (exactly) of the sample were transferred into the serum vial for DIC concentration. Vials were sealed with septa immediately and 2-3 mls were transferred into the serum vial for $\delta^{13}\text{C}$ -DIC. The rest of the vial was filled with N_2 sparged water. About 0.5 mls of headspace was left in the vial. Vials were sealed with Teflon septa immediately. 2 mls were transferred into the screw top vial for the ion analysis (SO_4^{2-} and Cl^-). The ion samples were refrigerated and DIC samples were frozen.

4. Ship Board Laboratory Analysis

a. Sulfate and Chloride Concentrations – Sulfate and chloride were measured with a Dionex DX-120 ion chromatograph equipped with an AS-9HC column. Samples were diluted 1:50 (vol/vol) prior to analysis and measured against a 1:50 diluted IAPSO standard seawater (28.9 mM SO_4^{2-} , 559 mM Cl^-). Concentrations were measured in pore waters of sediments from the

piston cores to assist in the prediction of hydrate beds below. For the estimation of the pore water sulfate methane interface (SMI) vertical sulfate profiles were plotted to observe the depth at which concentrations were measured below the ion chromatography limits of detection (<0.1 mM). The SMI is estimated to be the depth of the final measured concentration plus half the depth to the next section that pore water was sampled. For cores that sulfate profiles were not measured at zero the linear line for the decline in sulfate profiles was predicted to the t-intercept to estimate the SMI depth. Sulfate and chloride were measured against an IAPSO seawater standard and are presented in millimolar units (mM).

b. Pore Water Methane Concentrations - Methane concentrations were determined from 3-ml sediment plugs using headspace techniques and were quantified against certified gas standards (Scott Gas, Plumbsteadville PA). Headspace analysis was performed on board using a GC-FID Shimadzu GC-14A gas chromatograph equipped with a Hayesep 0.80/100 column. Methane concentrations are presented in millimolar units (mM).

c. Sulfide concentrations - Pore water sulfide concentrations were measured with a Turner spectrophotometer, using the Cline method (Cline, 1969). Sulfide concentrations are presented in millimolar units (mM).

5. Laboratory Analysis

a. Carbon Isotope Analysis - Stable carbon isotope ratios were measured on methane from gas pockets and pore water DIC. Radiocarbon analysis was performed on bulk sediment organic matter from select cores. For stable carbon isotope ($\delta^{13}\text{C}$) analysis, gases were analyzed with a Finnigan Delta S Isotope Ratio Mass Spectrometer with a sample injection through a Varian GC. For DIC, carbon dioxide was released into the headspace were by adding 100 μl of 10% HCl into the sample serum vial. Methane was oxidized to carbon dioxide prior to its introduction into the IRMS. Solid samples were analyzed using a CN combustion instrument with He carrier gas flowing into the isotope ratio mass spectrometer. For radiocarbon isotope analysis ($\Delta^{14}\text{C}$) samples in different carbon phases are combusted or acidified to CO_2 and concentrated in a cryogenic distillation line. The trapped CO_2 is converted to graphite for AMS analysis on the NRL system. Carbon dioxide was cryogenically purified and reduced to graphite at 575 $^\circ\text{C}$ in a hydrogen atmosphere using an iron catalyst. $\delta^{13}\text{C}$ and $\Delta^{14}\text{C}$ analysis is applied to trace the variation in sources, where the values are calculated as:

$$\delta^n C = \left[\frac{R_s}{R_{std}} - 1 \right] \times 1000 \text{ (‰)} \text{ (Eq. 1)}$$

where δ^n is the stable carbon isotope ratio, R is the $^{13}\text{C}/^{12}\text{C}$ for stable carbon $^{14}\text{C}/^{12}\text{C}$ for radiocarbon, s is the sample and std is the standard. For $\delta^{13}\text{C}$ analysis the standard is PeeDee Belmenite. For $\Delta^{14}\text{C}$ the standards are oxalic acid and ^{14}C dead coal. Radiocarbon was measured by AMS and is reported in the standard “per-mil” notation.

b. Pore Water DIC Concentrations - Pore water dissolved inorganic carbon (DIC) concentrations were measured using a UIC coulometer and standardized against a certified

reference material (CRM, Batch 58). DIC concentrations are presented in millimolar units (mM).

6. Heat Flow

High resolution heat flow data profiles were collected, processed and interpreted. NRL's telemetering marine heat-flow probe system, which was designed and built by the Geological Survey of Canada, measures temperature gradients and in-situ thermal conductivity of sediments both in lakes and coastal areas (water depth in 100's of metres) and in the deep ocean (water depths to 6000 metres). The length of probe was selected according to the "stiffness" of the sediments under investigation. NRL's probe is 3.5 meters long, penetrations were generally 3 meters. Temperatures and temperature gradients within the sediment were measured by thermistors that are located at known (30 cm) spacing within a small-diameter tube held in tension parallel to a solid steel strength member. Measurement of the thermal conductivity of the sediment was accomplished by allowing the probe to remain at rest in the sediment (typically for a period of 7 minutes) to allow dissipation of the frictional heating generated by the penetration of the probe, and then heating the probe and surrounding sediment by application of a known amount of energy (typically 600 joules/metre) to a heater wire paralleling the thermistors within the sensor tube. Analysis of the temperature decay following this period of energy input (or "heat pulse") yielded the conductivity of the sediment. Operation with a heat pulse at a study site took approximately 20 minutes.

Other parameters in addition to the temperatures in the probe were also logged. These include: pressure (water depth), water temperature, tilt, a stable reference resistance, and time. All parameters were logged in solid state memory.

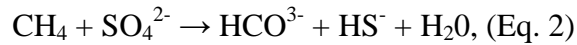
The probe was lowered at the beginning of a working day. After making a penetration into the sediments for thermal gradient measurements (and possibly a conductivity measurement), the probe was raised clear of the bottom and moved to the next site for another penetration. The probe was returned to the surface to download data after every third station. The probe continues to perform in this manner for a typical period of 12 hours, with operation during day light hours.

IV RESULTS

1. Piston Coring Geochemical Profiles

Field work commenced with piston coring to facilitate station selection and ensure heatflow probe penetration without damage. Coring site selection was intended to provide high resolution sulfate, methane, chloride, dissolved inorganic carbon, and DIC stable carbon isotope ratio data on and between mounds D and F. A combination of seismic data, heatflow profiles and pore water geochemistry data was utilized to predict regions that are abundant in deep sediment gas hydrates. Data from the seismic surveys is presented in the General Information section of this report. The geochemical and heatflow data will also be compared with the NRL DTAGS seismic survey planned for February 2005. Geochemical profiles are compared through the study region and then grouped according to the Chevron-Texaco JIP sites planned for investigation in Spring 2005.

Parameters for the pore water data include methane, sulfate, chloride and dissolved inorganic carbon concentration and stable carbon isotope ratio. Pore water geochemical data are plotted for comparison of methane and sulfate concentrations to assess the varying degrees of vertical methane fluxes and resulting methane oxidation (Borowski et al., 1999). Anaerobic methane oxidation occurs as:



in sediment depths were vertical flow of deep sediment methane and shallow sediment sulfate converge; i.e., sulfate-methane interface (SMI). This analysis is used to estimate the presence of methane deep in the sediments to provide an indication of gas hydrate potential. Dissolved inorganic carbon (DIC) is included to support the interpretation of methane oxidation to CO_2 by the anaerobic oxidation of methane (AOM). Stable carbon isotope analysis of the DIC provides additional interpretation of methane oxidation and contribution to the DIC pool. In biological oxidation of methane there is a difference in the enzyme activity in oxidation of ^{12}C and ^{13}C , where the rate for ^{12}C is more rapid and creates ^{13}C depleted stable carbon isotope signatures. Chloride data was originally incorporated to trace segments of the piston cores that contained hydrates with the assumption that chloride concentrations decrease in sections of the core that have dissociated hydrates through dilution by salt free melted hydrate. An alternate interpretation of the chloride data is presented below.

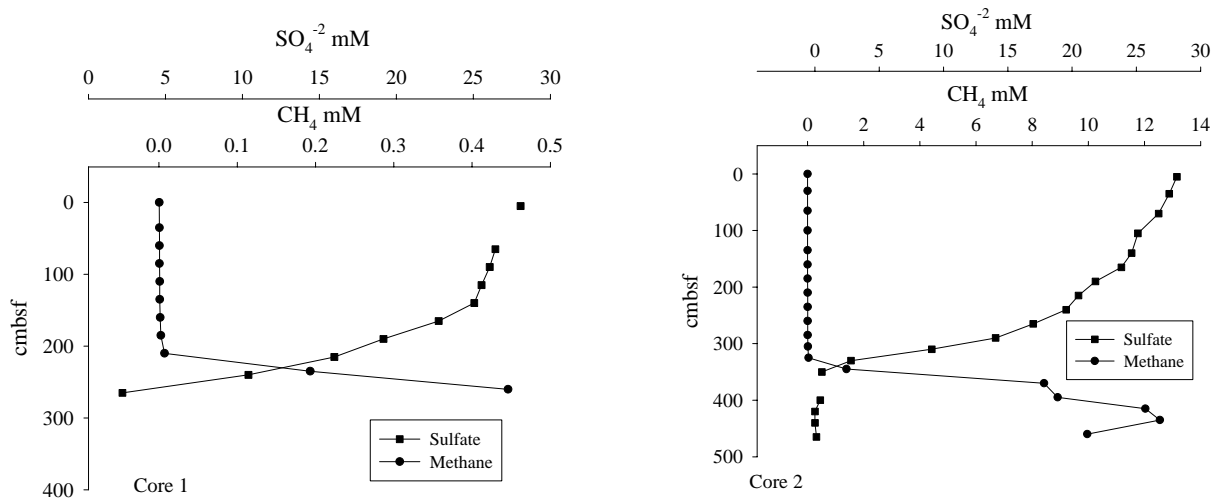


Figure 6: Piston core CH_4 and SO_4^{2-} profiles of stations located between the USGS seismic survey observation of mound D and mound F. Vertical profiles are presented as centimeters below sea floor (cmbsf).

Sulfate and methane data presented in the following figures are intended to provide an overview of the pore water profiles through the study region. The total data set is presented in Appendix 1. Based on data from the seismic survey Core 1 and Core 2 were selected as a control region in which low heatflow and gas flux were anticipated (Figure 6). The SMIs, estimated

from the sulfate profiles for Cores 1 and 2 were measured at 288 cm to 410 cm, respectively. Core 1 had lower methane concentrations, but the core was short and likely did not penetrate to a depth below the SMI. Sulfate gradients indicate a substantial methane flux. Core 2 penetrated the SMI and displays co-variation in methane and sulfate typical of cores with moderate gas flux.

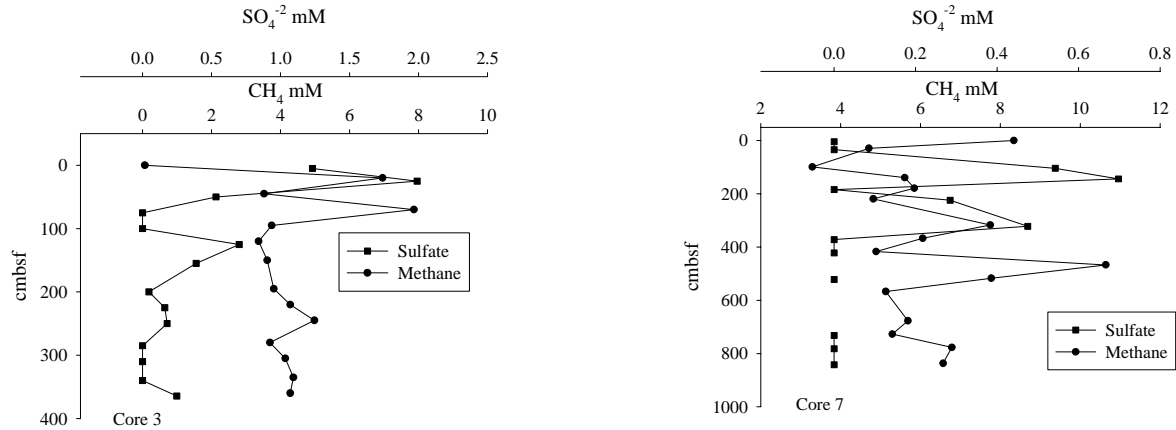


Figure 7: Piston core CH₄ and SO₄⁻² profiles of stations located on mound F that was identified on a USGS seismic survey. Vertical profiles are presented as centimeters below sea floor (cmbsf).

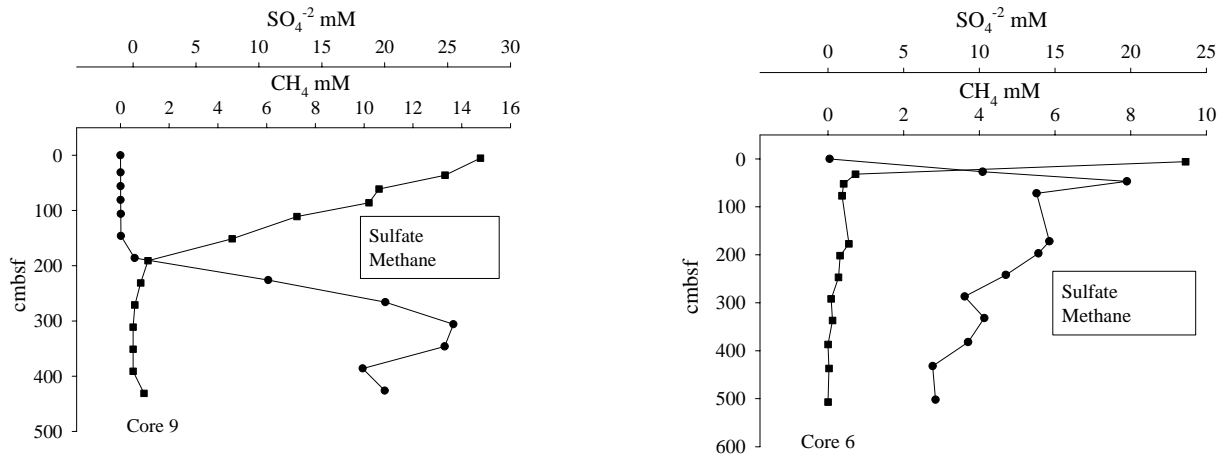


Figure 8: Piston core CH₄ and SO₄⁻² profiles of stations located to the north (core 6) and south (core 9) of mound F. Vertical profiles are presented as centimeters below sea floor (cmbsf).

Piston cores 3 and 7 were located on top of mound F (Figure 7). There was a remarkable difference in the pore water methane and sulfate profiles relative to Cores 1 and 2. In both cores sulfate was depleted near the sediment-water column interface. The range in sulfate concentrations was 0 to 0.70 mM for core 7 and 0 to 1.99 mM for core 3. Corresponding methane concentrations were elevated with values through the pore water profiles ranging from 3.29 to 10.6 mM for core 7 and 0.07 to 7.9 mM for core 3. The upward vertical flux of methane in these cores exceeds the downward flux of sulfate required to quantitatively oxidize the methane within the sediments. SMI depths in these cores were extremely shallow and likely extends to the sediment water interface.

Piston cores 6 and 9, located at the edge of the mound, displayed intermediate fluxes relative to the cores previously discussed. The SMI was estimated to be 45 cm for core 6 and 251 cm for core 9 (Figure 8).

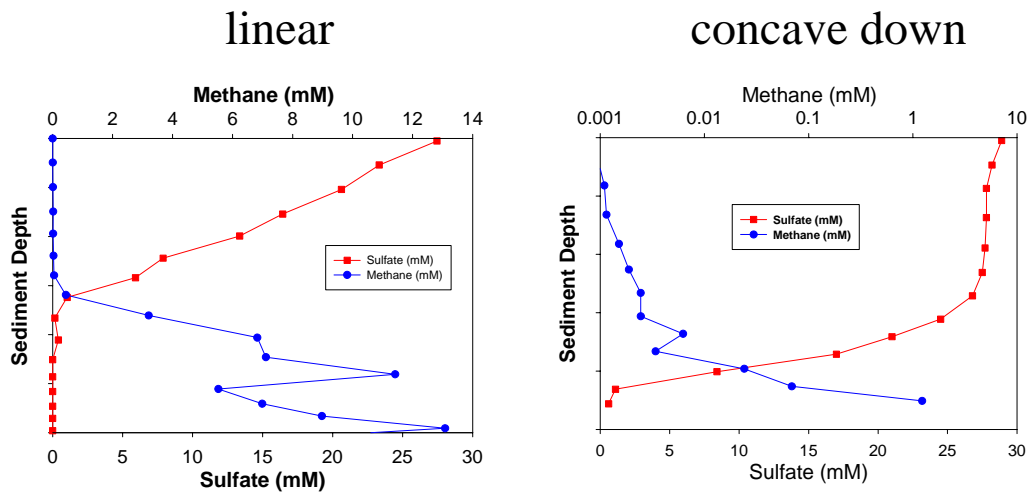


Figure 9: Example of piston core pore water data applied to predict deep sediment methane.

Pore water profiles of dissolved chemical constituents (in particular, sulfate) are useful for evaluating the biogeochemical conditions, gas flux and depositional history of a site. Under steady state conditions with high gas flux, “linear” sulfate profiles result due to diffusion and the anaerobic oxidation of methane (AOM) at the sulfate-methane interface (Figure 9). An alternate sulfate profile is a “concave down” concentration gradient (Figure 9). This type of curvature can result from changes in gas flux, downward vertical fluid advection, bioturbation or rapid sediment deposition. Non-linear profiles are transient features that will re-equilibrate once the perturbation ends. Sulfate profiles from piston cores on Atwater Valley sites were consistently concave down. Radiocarbon isotope analysis of the organic carbon from the cores will be used to assist in the interpretation of this profile shape.

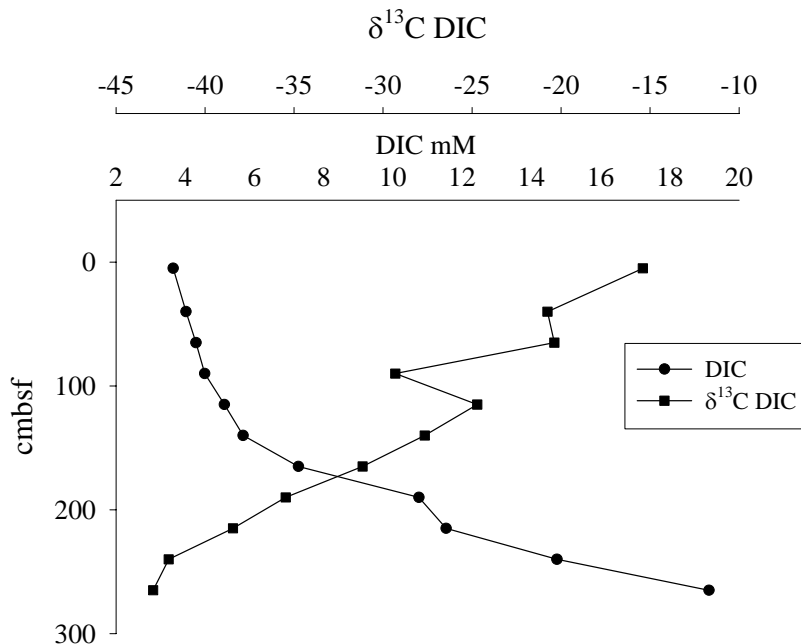


Figure 10: DIC concentration and $\delta^{13}\text{C}$ of DIC for Core 1 located in the center of the transect through Atwater Valley site between mound D and mound F. Vertical profiles are presented as centimeters below sea floor (cmbsf).

The concentration and $\delta^{13}\text{C}$ of pore water DIC mirrored the sulfate and methane data. Where there was depletion in the methane and sulfate pore water concentration, an increase in the DIC concentration and decrease in the $\delta^{13}\text{C}$ -DIC was observed. The control region, Core 1 had a deeper (but lower amplitude) increase in DIC concentration and decrease in the DIC $\delta^{13}\text{C}$ isotope signature (Figure 10). For core 7 the peak DIC concentration was 12.05 mM at 34 cm and core 2 was 19.54 mM at 340 cm. DIC concentration increases and $\delta^{13}\text{C}$ decreases ranged between 34 to 330 cm for cores 7 and 2, respectively (Figure 11). The differences noted between Cores 7 and 12 is due to higher rates of AOM in Core 7. The high shallow increases in the DIC concentration and depleted DIC $\delta^{13}\text{C}$ were dominant over mound F.

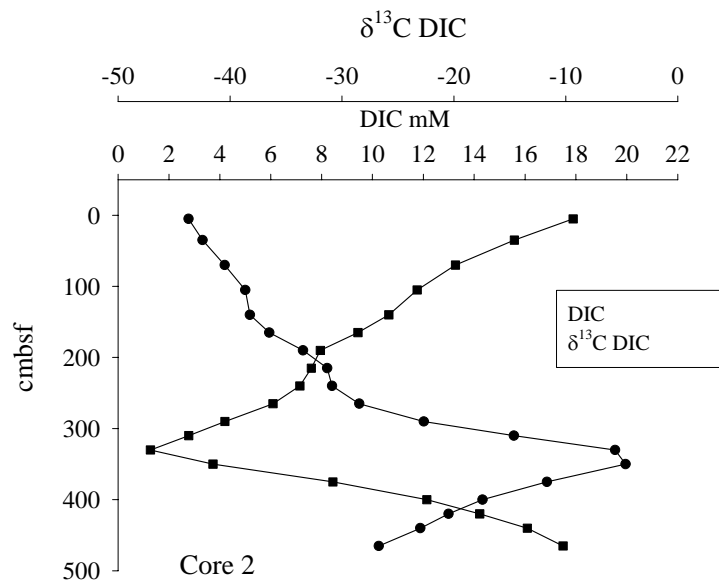
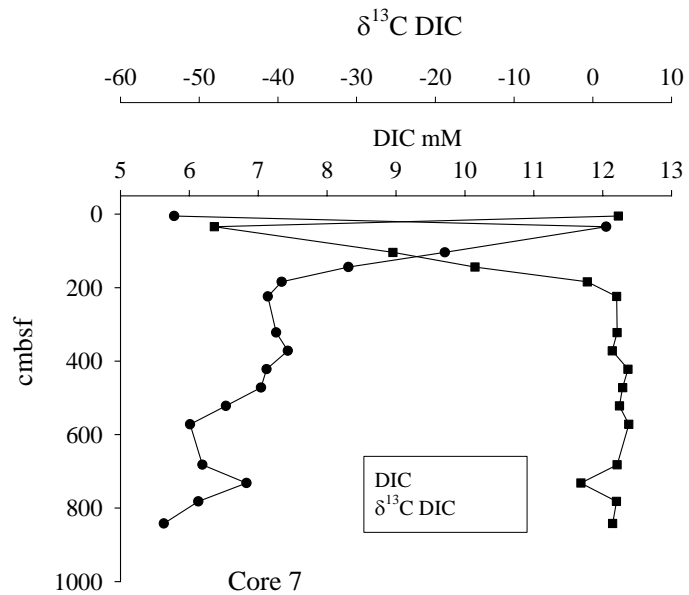


Figure 11: DIC concentrations and $\delta^{13}\text{C}$ of DIC for Core 7 and Core 2 present the range in profiles taken during the Atwater Valley survey. Vertical profiles are presented as centimeters below sea floor (cmbsf).

Pore water chloride concentrations were measured to provide an indication of dissociated gas hydrates. Chloride concentrations below seawater (559 mM) indicate hydrates may have dissociated and diluted the pore water. Among the 15 cores we analyzed (Figure 12), pore water freshening was observed in one sample from one core (Core 9). Instead, chloride concentrations higher than seawater were measured in many of the cores. Cores distal to mound F had background chloride concentrations, (e.g. cores 1, 2, 5, 9, 10, 12, 13, 14 and 15). Intermediate

chloride concentrations were observed in cores 6, 11 and 8 (near and on mound F). The highest chloride concentrations were observed in Cores 3, 7 and 4, which were collected directly over the mound. This trend indicates a vertical flux of fluid affected by the deeper salt diapers. This interpretation is consistent with that based on the sulfate and methane data described previously and the heatflow data presented below.

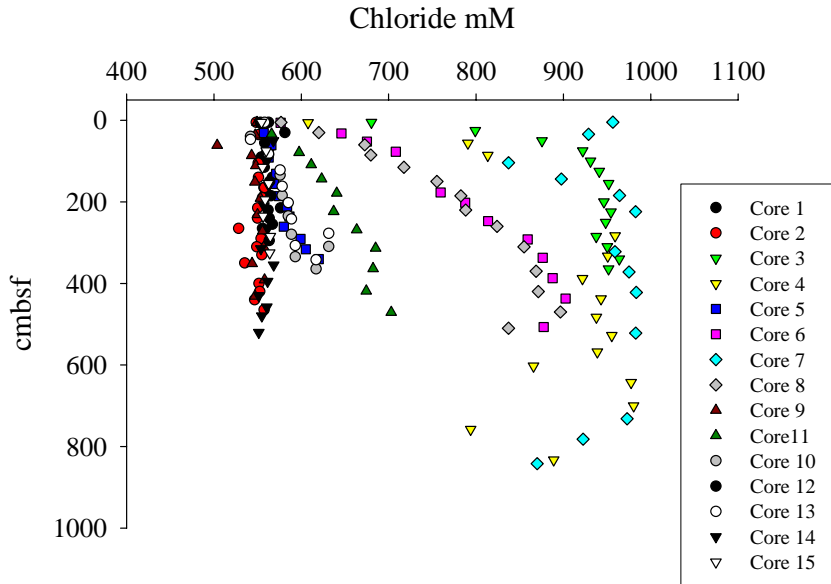


Figure 12: Chloride profiles for piston core pore water samples. Vertical profiles are presented as centimeters below sea floor (cmbsf).

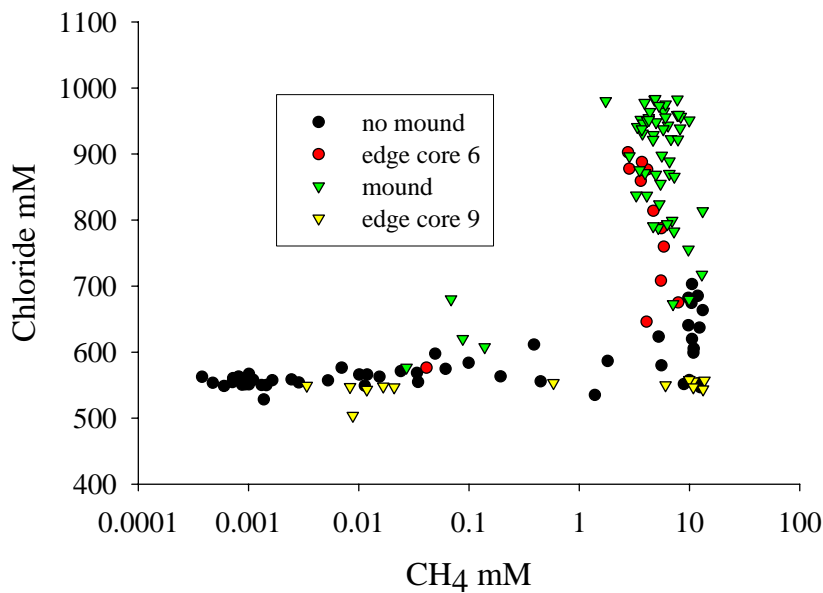


Figure 13: Comparison of pore water methane and chloride concentrations from cores on top of, on the edge and away from mound F. Vertical profiles are presented as centimeters below sea floor (cmbsf).

Further analysis of chloride shows a large variation relative to pore water methane concentrations (Figure 13). Cores from mound F had a high concentration of methane and chloride in pore water samples, while cores off the mound had typical background chloride with a large range in the methane concentrations; some samples with concentrations as high as values measured on mound samples. Cores 6 and 9 were located at the edge of the mound and were diverse in the pore water methane and chloride concentrations; core 9 data was similar to coring sites off the mound and core 6 data was similar to cores taken from the mound. This result suggests that regions with a high vertical flow of methane and chloride are sites where the pore water chloride, from the salt mounds, decreases the hydrate stability and increases the pore water methane concentration. This observation will assist in data interpretation and deep core drilling site selection by the Chevron-Texaco JIP program in this region.

Table 3: Core gas methane $\delta^{13}\text{C}$ data. Additional information includes vertical location of the gas pocket in the core, gas retention time (Rt) in the GC run and the area for the mass 44 peak. Standard deviations were calculated for samples from 180 cm in core 3 and 567 cm in core 7.

Core	Corrected distance from top of core (cm)	Component	Rt	$\delta^{13}\text{C}$	Area 44	average	stdev
3	180	CH4	121.8	-72.373	66.049	-72.4623	0.098521
3	180	CH4	122.1	-72.568	19.279		
3	180	CH4	122.7	-72.446	18.605		
3	203	CH4	122.3	-71.956	17.222		
3	222	CH4	122.3	-72.429	11.221		
3	246	CH4	122.3	-72.077	21.241		
4	615	CH4	121.8	-71.104	15.528		
4	670	CH4	122.3	-71.323	20.165		
4	715	CH4	122.3	-71.84	15.042		
6	309	CH4	122.3	-63.736	14.755		
6	321	CH4	122.3	-67.984	12.113		
7	567	CH4	121	-71.206	40.998	-71.272	0.088831
7	567	CH4	122.7	-71.373	19.641		
7	567	CH4	122.1	-71.237	19.558		
7	742	CH4	122.3	-69.224	24.168		
8	240	CH4	122.5	-65.842	13.261		
8	275	CH4	122.1	-70.851	21.197		
8	362	CH4	122.7	-72.271	24.419		
9	400	CH4	122.1	-79.878	15.662		
11	242	CH4	122.5	-68.964	14.067		
11	372	CH4	122.3	-76.418	17.152		

Gas from the expansion cracks in the core liner was microbial in origin. Table 3 presents gas samples obtained from cores 3, 4, 6, 7, 9, and 11. The $\delta^{13}\text{C}$ of the methane ranged from -79.88‰ to -63.74‰. The variation suggests different degrees of microbial methane production and oxidation in the sediments and/or slight inputs of from thermogenic sources. Trace quantities of propane were detected in several cores. The average methane/ethane ratio for all

pore water was 866. These data are also consistent with a microbial gas origin with a possible slight contribution from a thermogenic source. Further understanding of variation in $\delta^{13}\text{C}$ of the methane will be accomplished with analysis of pore water methane and DIC.

2. Data Comparison of Chevron-Texaco JIP sites

One of the missions for this research cruise was to provide baseline data for the Chevron-Texaco JIP hydrate deep drilling plans on Atwater Valley. Fieldwork was designed to combine seismic, heatflow and piston coring data at the planned drilling sites. Piston cores 3, 1, 2, 15 and 7 corresponding, respectively, to the JIP sites 1, 2, 3, 4, and 5 are compared to pore water profiles in the following data presentation. The JIP sites 1 and 5 were located on mound F, JIP 2 and 5 were on the transect line between mounds D and F, and JIP 4 was on mound D.

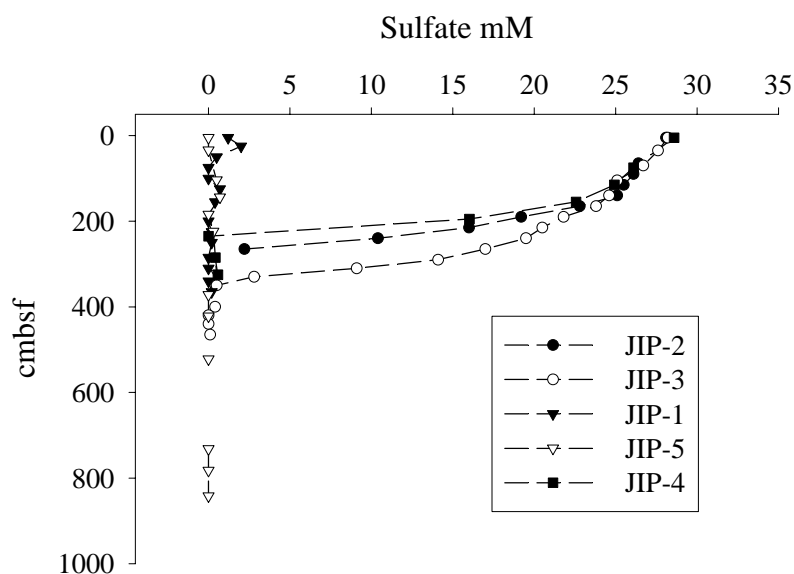


Figure 14: Pore water sulfate concentration profiles plotted relative to centimeters below the sea floor (cmbsf) for JIP sites along the Atwater Valley transect between mounds D and F.

Pore water sulfate concentrations were divided in two distinct profiles for the JIP sites (Figure 14). Sulfate was depleted through the piston cores at JIP-1 and JIP-5, suggesting anaerobic oxidation of methane and reduction of sulfate at the sediment-water column interface. Sulfate penetrated deeper at JIP-2, JIP-3 and JIP-4. For these cores the SMI ranged from 218 cm to 410 cm (Appendix 1). The JIP-1 and JIP-5 stations, on mound F, appear to have the highest methane flux.

Pore water methane concentrations matched the sulfate profiles measured in the JIP stations (Figure 15). At JIP-1 and JIP-5, on mound F, methane concentrations were high through the vertical profile to the water column-sediment interface, ranging from 0.1 mM to 10.6 mM, with an average of 5.3 mM. At JIP-2, JIP-3 and JIP-4 methane profiles were depleted from approximately 300 cm to the sediment surface and averaged 1.5 mM. The high concentrations are a result of the high methane flux, with sulfate concentrations that did not provide an electron acceptor in the anaerobic oxidation of methane.

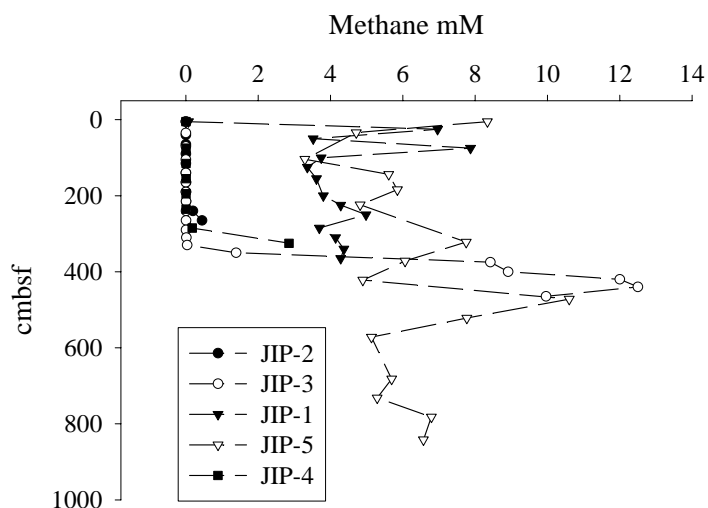


Figure 15: Pore water methane concentration profiles plotted relative to centimeters below the sea floor (cmbsf) for JIP sites along the Atwater Valley transect between mounds D and F.

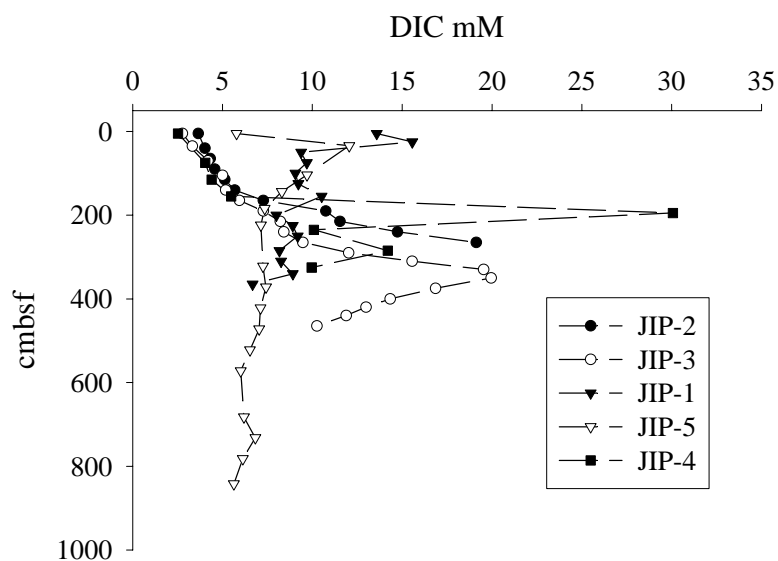


Figure 16: Pore water DIC concentration profiles plotted relative to centimeters below the sea floor (cmbsf) for JIP sites along the Atwater Valley transect between mounds D and F.

Pore water DIC profiles are presented in Figure 16. Surface concentrations, above 200 cm in these two locations are distinctly different. JIP-1 and JIP-5, which are located on top of mound F, have greater concentration, ranging between 2.8 mM and 15.6 mM. The other three locations were found to be at concentrations that were less than 5 mM. Higher concentrations on the mound correspond to the methane and sulfate profiles at these sites which indicate high methane vertical flow and active anaerobic methane oxidation.

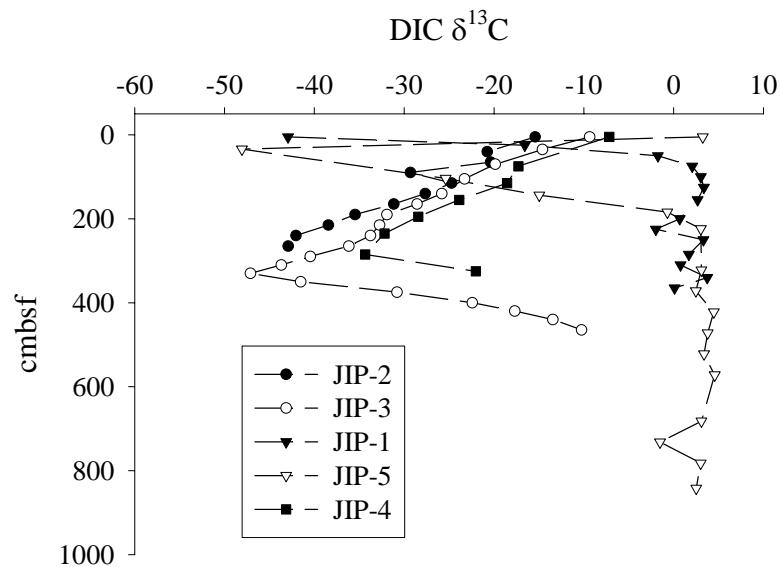


Figure 17: Pore water dissolved inorganic carbon concentration profiles plotted relative to centimeters below the sea floor (cmbsf) for JIP sites along the Atwater Valley transect between mounds D and F.

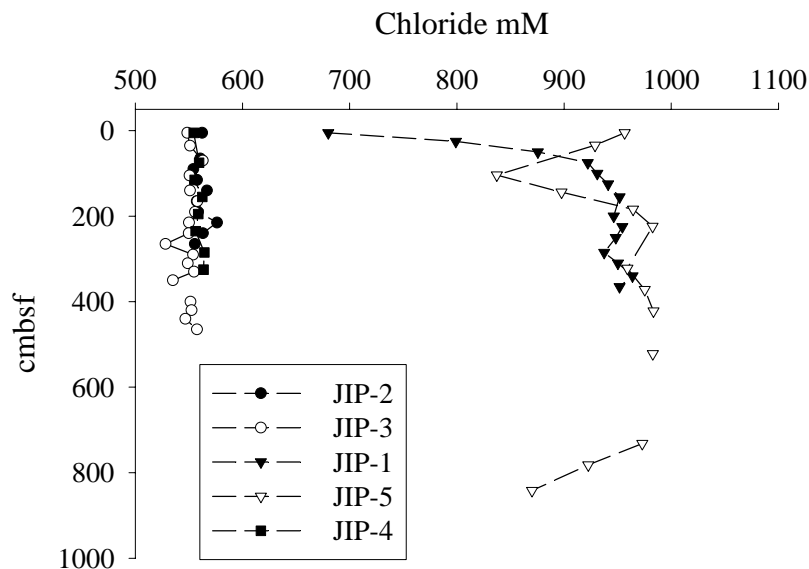


Figure 18: Pore water chloride concentration profiles plotted relative to centimeters below the sea floor (cmbsf) for JIP sites along the Atwater Valley transect between mounds D and F.

Stable carbon isotope analysis of the pore water DIC is used for further explanation of the methane cycling (Figure 17). With higher vertical methane flow on mound F at the JIP-1 and JIP-5 locations, there are ^{13}C depleted isotope signatures which indicate active anaerobic oxidation of methane. The ^{13}C -depleted signatures at JIP-2, JIP-3 and JIP-4 are deeper in the piston cores, suggesting less methane flux in regions, relative to JIP-1 and JIP-5.

Chloride concentrations at the JIP sites do not show significant decrease from values ranging around 550 mM (Figure 18). In contrast, the JIP-1 and JIP-3 sites on mound F are enriched in chloride. These data suggest high salt diffusion in pore water from salt diapirs below the mound.

C. Heatflow Survey

Heat flow measurements were made along the NW-SE USGS seismic line that crossed both mound D and mound F. With the exception of HF4 and HF7, located on the summit of mound F, the thermistors at depths of less than about 1 meter recorded equilibrium sediment temperatures that deviate significantly from the expected linear trend (Figures 19 and 20). The cause of this curvature in the temperature profile, with shallow temperatures warmer than expected, is unknown, but could result from a recent spurt of increased sedimentation or a recent slight (0.05 degrees C) increase in bottom water temperature. Increased sedimentation could be in the form of a thin recent slump deposit or turbidite. Abrupt temperature changes could occur beneath the warm eddies that are periodically spun off by the Gulf Loop Current and drift westward across the northern Gulf (Hamilton, 1990). These eddies are known to affect bottom circulation patterns in this area (Hamilton, 1990).

Heat flow values were determined at each station by computing thermal resistance values at each thermistor,

$$R = \int (1/\lambda) dz, \text{ (Eq. 3)}$$

where λ is the thermal conductivity. In a situation of steady-state conductivity the heat flow is equal to the slope of the line on a Bullard Plot, a plot of temperature vs. thermal resistance. For each station, the non-linear data from depths of less than 0.9 meters was removed, and the heat flow value determined from the slope of the best-fitting linear least-squares line through the remaining data. All heat flow values were corrected for instrument tilt (all tilt values were less than 5.4 degrees, requiring corrections of less than 0.45%).

The data show clear anomalies in sediment temperature and heat flow associated with the mounds. Measurements collected on the top of mound F show elevated sediment temperatures, and heat flow values of around 160 mW/m². Sediment temperatures decrease away from the summit of the mound, and heat flow values drop to a background level of 40 to 50 mW/m² (Figures 20 and 21). Sediment temperatures at the summit of mound D are similar to what was observed at mound F, and heat flow values are slightly lower at around 132 mW/m², partly as a result of the slightly higher bottom water temperature and thus reduced thermal gradient. Away from the summit of mound D the thermal gradient decreases and heat flow values drop to around 50 mW/m².

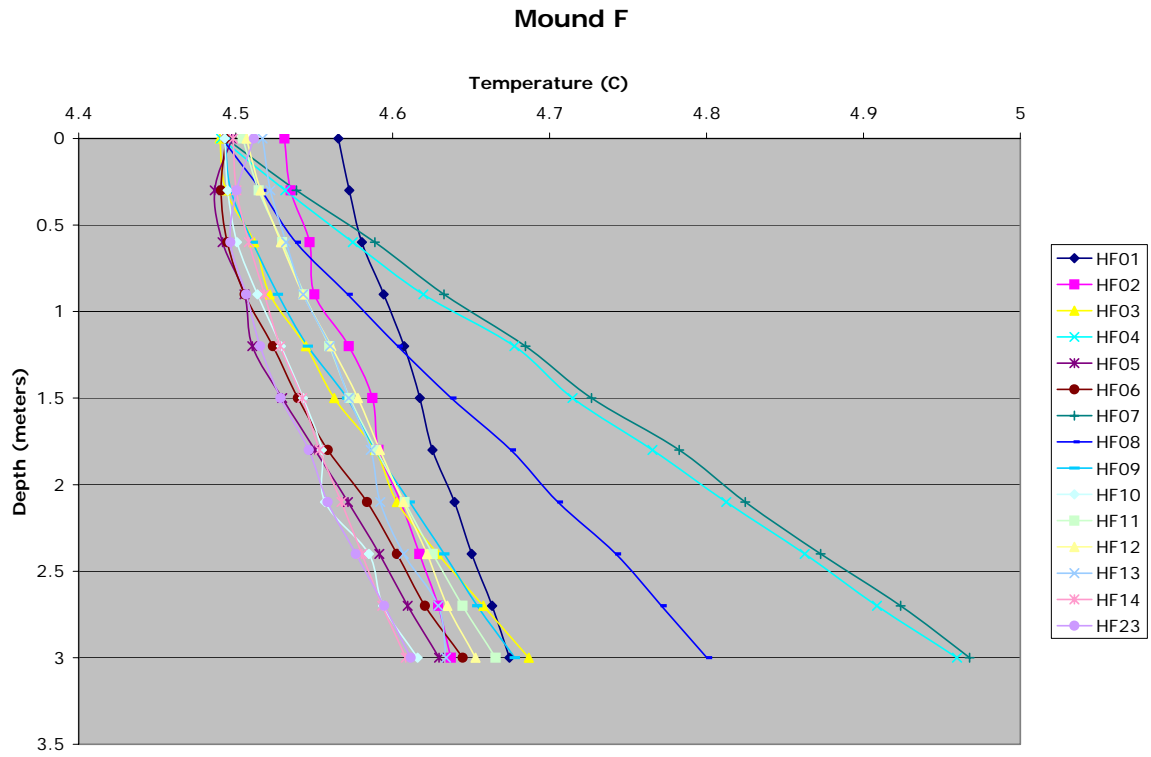


Figure 19: Temperature vs. Depth plots for stations along transect over Mound F.

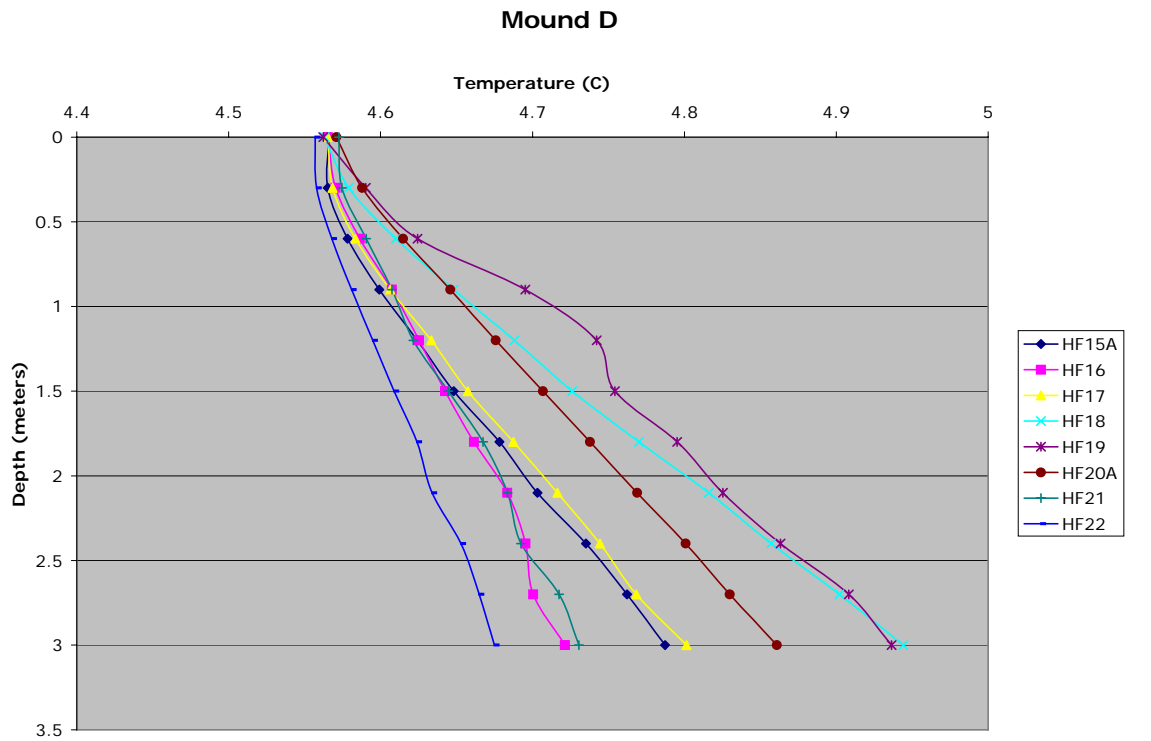


Figure 20. Temperature vs. depth plots for stations along transect over Mound D.

Thermal Profile

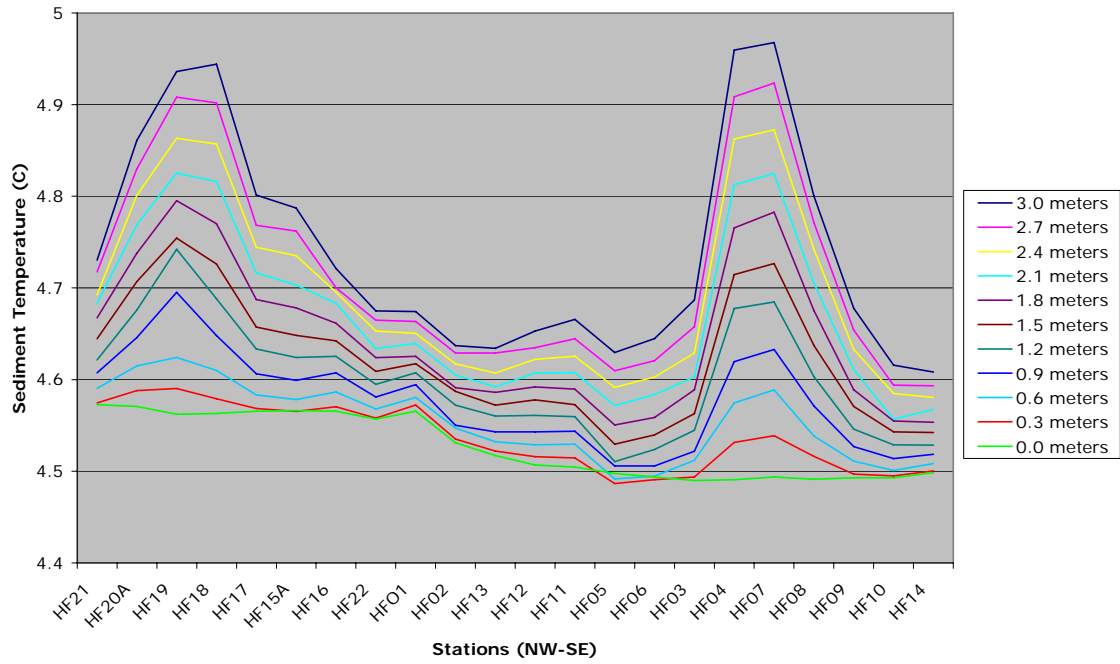


Figure 21. Thermal profiles for all thermistors along the entire transect.

Heat Flow Profile

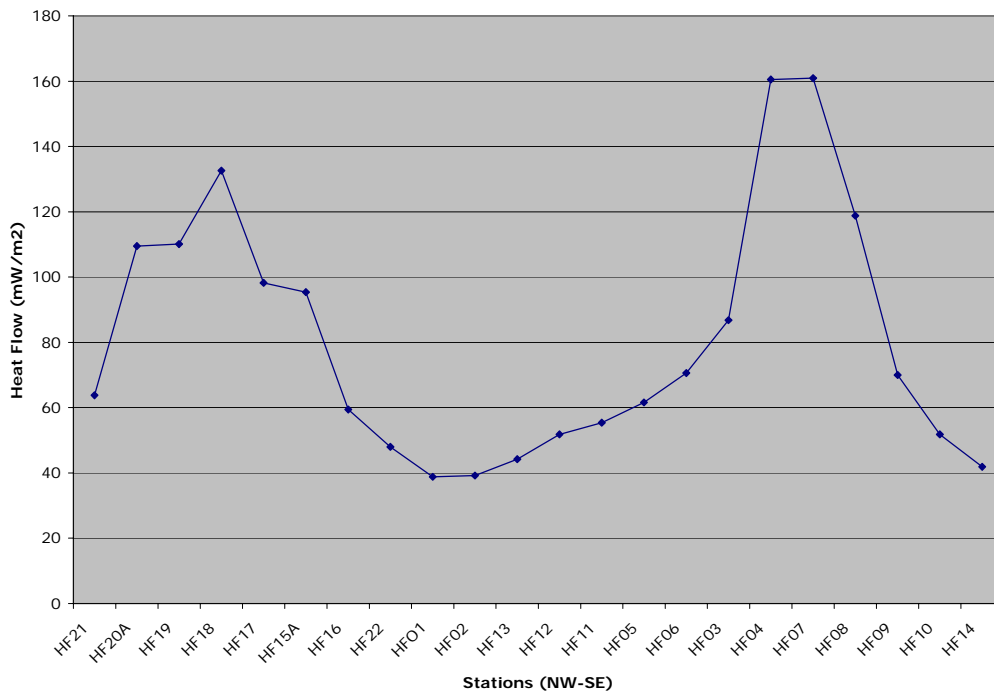


Figure 22. Heat flow profile for all stations along the transect from mound D to mound F.

V. SUMMARY

The following points are a general summary of the preliminary data review of the Atwater Valley research cruise. The data interpretation presented in this report will be revised with analyses that are being completed in the laboratory.

1. Geochemical analysis of sulfate and methane from piston core pore water samples shows a deeper SMI between mounds D and mound F. However, relative to other locations, the depth of the SMI between the mounds is shallow (Borowski et al., 1999).
2. Sulfate and methane pore water profiles from piston cores on mound F were found to have the largest vertical methane flux. Sulfate was depleted in surface core samples and methane concentrations were elevated, which suggests a flux of methane into the water column.
3. Research exploration of methane hydrates was conducted with a comparison of Keathley Canyon and Atwater Valley. The average SMI for Keathley Canyon was substantially deeper than Atwater Valley in the piston cores, with average values of 541 ± 155 mM (n=18) vs. 270 ± 132 mM (n=12), respectively. Also, data were not available from three of the cores on Atwater Valley because the high vertical methane flux inhibited sulfate data interpretation. Deep drilling conducted by during the Chevron-Texaco JIP will determine if the greater vertical methane flux measured at Atwater Valley results from greater pore water methane concentration from the hydrate bed because of more abundance of hydrates or greater hydrate dissociation and methane release resulting from the increases in pore water salinity caused by salt mounds in this region.
4. Stable carbon isotope and gas composition sampled from the piston cores has a predominately a microbial methane source. This is an interesting finding relative to identification of thermogenic methane in Atwater Valley at a depth of 1900 m to the south of mound F (Sassen et al., 2001). Future field surveys are needed for understanding local variation in the hydrate gas source(s).
5. Chloride data from piston cores did not indicate the presence of hydrates. However, high chloride concentrations were measured on mound F and may have masked the pore water freshening signal imparted during the dissociation of gas hydrate. It is expected that the chloride originates from deep salt mounds. This supports observation of vertical methane flow in this region.
6. DIC concentrations and stable carbon isotope analysis confirm anaerobic methane oxidation in the pore water profiles. Mound F sites show more shallow increases in DIC concentration and ^{13}C depleted DIC pools, indicating an increased vertical methane flow.
7. Data from the proposed Chevron-Texaco JIP deep well drilling sites was independently evaluated. Chevron-Texaco sites JIP-1 and JIP-5 are located on mound F. Methane, sulfate, chloride, DIC and DIC $\delta^{13}\text{C}$ all indicate this region is the most active in vertical methane flux. Sites JIP-2, JIP-3 and JIP-4 had deeper SMIs, but still indicate substantial

methane flux and are shallow relative to 10 m to 100 m SMI reported in other coastal regions (Borowski et al., 1999).

8. Through the region cored there is a large variation between the methane and chloride concentrations measured away from mound F, at the base of mound F and on top of mound F. With the high correlation between chloride and methane concentrations indicating a decrease in hydrate stability resulting from salt diapir mineral flow into the pore water these data will assist in selection of the deep drill locations and data interpretation.
9. The data show clear anomalies in sediment temperature and heat flow associated with the mounds. Measurements collected on the top of mound F show sediment temperatures elevated by 0.3°C relative to the surrounding seafloor, and heat flow values of around 160 mW/m^2 . Sediment temperatures decrease away from the summit of the mound, and heat flow values drop to a background level of 40 to 50 mW/m^2 . Sediment temperatures at the summit of Mound D are similar to what was observed at Mound F, and heat flow values are slightly lower at around 132 mW/m^2 , partly as a result of the slightly higher bottom water temperature and thus reduced thermal gradient.
10. Data from the Atwater Valley piston coring and heat flow show similar active regions for vertical methane flow.

VI. FUTURE GOALS

1. The geochemical and heatflow data is being compared with the NRL DTAGS seismic survey of this region that is planned for February 2005. These data will be used to plan future methane hydrate surveys in the Gulf of Mexico, on the Texas-Louisiana Shelf.
2. Radiocarbon isotope analysis of sediment organic carbon may provide a better understanding of the existing data.
3. The data base will be reviewed for planning future seismic, coring and heatflow surveys of this region.
4. Data will be provided to the Chevron-Texaco JIP for planning and interpretation of the deep drilling in this region.
5. Current and future data will be compiled for peer review manuscript(s).

VII. ACKNOWLEDGMENTS

This research cruise received strong support in the piston coring site selections from the seismic profiles provide by Drs. Deborah Hutchinson and Patrick Hart, US Geologic Survey. We appreciate the assistance in coring and heatflow data collection provided by the crew of the RV Gyre. This research was funded by DOE/NETL, ONR and NRL.

VIII. LITERATURE CITED

Borowski, W. S., C. K. Paull, and W. Ussler III. 1999. Global and local variations of interstitial sulfate gradients in the deep-water, continental margin sediments: Sensitivity to underlying methane and gas hydrates. *Mar. Geol.* 159:131-154.

Cline, J. D. 1969. Spectrophotometric Determination of Hydrogen Sulfide in Natural Waters. Pp. 454-458, *Limnology and Oceanography*.

Hamilton, P., Deep Currents in the Gulf of Mexico, 1990 *Journal of Physical Oceanography*, Vol 20, p 1087-1104.

Hyndman, R.D., Davis, E.E., and Wright, J.A., The measurement of marine geothermal heat flow by a multipenetration probe with digital acoustic telemetry and insitu thermal conductivity, *Marine Geophys. Res.*, 4, 181-205, 1979.

Sassen, R., S. T. Sweet, D. A. DeFreitas, J. A. Morelos, A. V. Milkov. 2001. Gas hydrate and crude oil from the Mississippi Fan Foldbelt, downdip Gulf of Mexico Salt Basin: significance to petroleum system. *Org. Geochem.* 32:999-1008.

Villinger, H., and Davis, E.E., A new reduction algorithm for marine heat flow measurements, *J. Geophys. Res.*, 92, 12,846-12,856, 1987.

APPENDIX 1: Pore water data summary from Atwater Valley piston coring.

GOM_JIP_2 Cruise, May 2004										
Pore Water Data										
Core	Syringe	Pore Water Depth Below Surface (cm)	Chloride (mM)	Sulfate (mM)	DIC (mM)	$\delta^{13}\text{C-DIC}$	Gas Sample Depth Below Surface (cm)	Gas Sample #	CH4 (mM)	SMI (cm)
1	C011	5	562.5	28.1	3.6	-15.4	0	11	3.79E-04	288
1	C010	40			4.0	-20.8	35	10	5.31E-04	
1	C009	65	560.6	26.4	4.3	-20.4	60	9	7.24E-04	
1	C008	90	554.2	26.1	4.6	-29.3	85	8	7.16E-04	
1	C007	115	557.6	25.5	5.1	-24.7	110	7	8.75E-04	
1	C006	140	566.9	25.1	5.7	-27.7	135	6	1.01E-03	
1	C005	165	557.3	22.8	7.3	-31.1	160	5	1.64E-03	
1	C004	190	558.5	19.2	10.8	-35.5	185	4	2.45E-03	
1	C003	215	576.3	16.0	11.5	-38.4	210	3	7.00E-03	
1	C002	240	563.1	10.4	14.7	-42.0	235	2	1.93E-01	
1	C001	265	555.5	2.2	19.1	-42.9	260	1	4.46E-01	
2	C030	5	548.5	28.2	2.8	-9.4	0	30	6.00E-04	410
2	C029	35	551.1	27.6	3.3	-14.6	30	29	9.34E-04	
2	C028	70	562.9	26.7	4.2	-19.9	65	28	8.13E-04	
2	C027	105	550.6	25.1	5.0	-23.3	100	27	8.73E-04	
2	C026	140	551.0	24.6	5.2	-25.8	135	26	1.01E-03	
2	C025	165	557.9	23.8	5.9	-28.6	160	25	1.10E-03	
2	C024	190	555.7	21.8	7.3	-31.9	185	24	1.00E-03	
2	C023	215	550.1	20.5	8.2	-32.7	210	23	1.31E-03	
2	C022	240	549.9	19.5	8.4	-33.8	235	22	1.45E-03	
2	C021	265	528.3	17.0	9.5	-36.2	260	21	1.38E-03	
2	C020	290	553.9	14.1	12.0	-40.4	285	20	2.86E-03	
2	C019	310	549.0	9.1	15.6	-43.7	305	19	1.13E-02	
2	C018	330	554.8	2.8	19.5	-47.1	325	18	3.46E-02	
2	C017	350	535.1	0.5	20.0	-41.5	345	17	1.39E+00	
2	C016	375	547.7	0.9	16.9	-30.8	370	16	8.42E+00	
2	C015	400	551.5	0.4	14.3	-22.4	395	15	8.91E+00	
2	C014	420	552.5	0.0	13.0	-17.7	415	14	1.20E+01	
2	C013	440	546.7	0.0	11.9	-13.4	435	13	1.25E+01	
2	C012	465	557.5	0.1	10.3	-10.3	460	12	9.96E+00	
3	C044	5	680.1	1.2	13.6	-42.9	0	44	6.87E-02	no SMI
3	C043	25	799.1	2.0	15.6	-16.6	20	43	6.96E+00	
3	C042	50	875.5	0.5	9.4	-1.8	45	42	3.52E+00	
3	C041	75	922.1	0.0	9.7	2.1	70	41	7.87E+00	
3	C040	100	931.0	0.0	9.1	3.0	95	40	3.74E+00	
3	C039	125	941.0	0.7	9.2	3.4	120	39	3.36E+00	
3	C038	155	951.8	0.4	10.5	2.7	150	38	3.61E+00	
3	C037	200	946.3	0.0	8.0	0.7	195	37	3.80E+00	
3	C036	225	954.4	0.2	8.9	-2.0	220	36	4.28E+00	
3	C035	250	948.3	0.2	9.2	3.3	245	35	4.98E+00	
3	C034	285	937.5	0.0	8.2	1.7	280	34	3.69E+00	
3	C033	310	950.3	0.0	8.3	0.8	305	33	4.14E+00	
3	C032	340	963.9	0.0	8.9	3.7	335	32	4.37E+00	
3	C031	365	951.7	0.2	6.7	0.1	360	31	4.28E+00	
4	C059	6	607.7	9.8	10.9	-51.1	0	59	1.39E-01	no SMI
4	C058	56	790.7	3.1	9.5	-17.5	46	58	4.69E+00	
4	C057	86	813.4	4.9	8.5	-7.8	66	57	1.32E+01	

4	C056	283	959.2	0.4	7.7	10.8	278	56	7.94E+00	
4	C055	333	950.8	0.2	7.6	6.2	328	55	9.95E+00	
4	C054	388	921.8	0.5	7.3	4.4	383	54	4.68E+00	
4	C053	438	943.2	1.2	7.3	4.6	433	53	6.40E+00	
4	C052	483	937.8	1.0		0.7	478	52	5.79E+00	
4	C051	528	955.5	0.3	7.2	5.8	523	51	6.05E+00	
4	C050	568	939.0	0.1	6.7	4.7	563	50	8.21E+00	
4	C049	603	865.8	0.0	6.2	5.6	598	49	7.29E+00	
4	C048	643	977.6	0.0	6.9	6.0	638	48	3.92E+00	
4	C047	701	980.3	0.0	6.9	0.4	693	47	1.74E+00	
4	C046	758	793.9	0.0	5.9	3.5	753	46	6.28E+00	
4	C045	833	888.9	0.0	5.8	4.6	828	45	6.58E+00	
5	C072	5	553.4	28.5	2.6	-6.8	0	72	4.75E-04	224.0
5	C071	31	557.0	22.4	5.5	-33.3	26	71	5.27E-03	
5	C070	61	565.8	20.0	7.1	-38.7	56	70	1.01E-02	
5	C069	91	562.6	17.2	9.2		86	69	1.54E-02	
5	C068	131	571.2	14.2	10.1	-43.3	126	68	2.41E-02	
5	C067	156	568.6	15.7	11.5	-45.6	151	67	3.37E-02	
5	C066	186	574.5	12.0	12.8	-45.4	181	66	6.15E-02	
5	C065	211	583.6	8.0	15.1	-49.4	206	65	9.93E-02	
5	C064	236	586.5	0.0	13.9	-48.3	231	64	1.81E+00	
5	C063	261	579.9	0.1	18.1	-32.0	256	63	5.57E+00	
5	C062	291	599.2	0.8	15.8	-21.1	286	62	1.08E+01	
5	C061	316	605.2	0.0	14.0	-11.9	311	61	1.09E+01	
5	C060	341	619.9	0.0	11.0	-6.2	336	60	1.05E+01	
6	C084	6	576.3	23.6	5.2	7.3	0	84	4.11E-02	45.0
6	C083	32	645.9	1.8	14.2	7.9	27	83	4.09E+00	
6	C082	52	675.2	1.0	13.0	7.3	47	82	7.90E+00	
6	C081	77	708.2	0.9	12.6	5.9	72	81	5.51E+00	
6	C080	177	759.5	1.4	12.6	3.6	172	80	5.85E+00	
6	C079	202	787.6	0.8	11.3	-0.7	197	79	5.56E+00	
6	C078	247	813.8	0.7	12.6	-6.1	242	78	4.70E+00	
6	C077	292	859.1	0.2	10.6	-12.2	287	77	3.61E+00	
6	C076	337	876.4	0.3	11.1	-25.0	332	76	4.13E+00	
6	C075	387	887.7	0.0	10.3	-36.1	382	75	3.70E+00	
6	C074	437	902.5	0.1	10.1	-45.2	432	74	2.77E+00	
6	C073	507	877.5	0.0	8.6	-31.8	502	73	2.84E+00	
7	C100	5	956.5	0.0	5.8	3.2	0	100	8.34E+00	no SMI
7	C099	34	928.9	0.0	12.1	-48.1	29	99	4.71E+00	
7	C098	104	837.2	0.5	9.7	-25.4	99	98	3.29E+00	
7	C097	144	897.6	0.7	8.3	-15.0	139	97	5.61E+00	
7	C096	184	964.3	0.0	7.3	-0.7	179	96	5.85E+00	
7	C095	224	982.6	0.3	7.1	3.0	219	95	4.82E+00	
7	C094	322	959.1	0.5	7.3	3.1	317	94	7.75E+00	
7	C093	372	975.2	0.0	7.4	2.5	367	93	6.06E+00	
7	C092	422	983.4	0.0	7.1	4.5	417	92	4.89E+00	
7	C091	472	953.0	0.0	7.0	3.8	467	91	1.06E+01	
7	C090	522	982.8	0.0	6.5	3.4	517	90	7.77E+00	
7	C089	572	924.1	0.0	6.0	4.6	567	89	5.13E+00	
7	C088	682	876.9	0.0	6.2	3.1	677	88	5.69E+00	
7	C087	732	973.0	0.0	6.8	-1.5	727	87	5.29E+00	
7	C086	782	922.6	0.0	6.1	3.0	777	86	6.79E+00	
7	C085	842	870.1	0.0	5.6	2.5	837	85	6.57E+00	
8	T014	5	576.8	21.9	5.5	-38.3	0	114	2.71E-02	59.0
8	T013	30	620.0	8.3	11.3	-54.7	25	113	8.76E-02	

8	T012	60	672.7	1.5	13.8	-44.3	55	112	7.10E+00	
8	T011	85	679.6	1.3	12.1	-37.9	80	111	9.92E+00	
8	T010	115	717.5	1.0	12.0	-29.3	110	110	1.30E+01	
8	T009	150	755.2	0.3	11.5	-18.1	145	109	9.77E+00	
8	T008	185	782.7	0.3	11.2	-7.4	180	108	7.23E+00	
8	T007	220	788.1	0.6	11.5	-4.7	215	107	5.21E+00	
8	T006	260	824.0	0.3	9.8	0.2	255	106	5.32E+00	
8	T005	310	854.9	0.1	10.8	2.0	305	105	5.46E+00	
8	T004	370	868.8	0.1		3.8	365	104	4.96E+00	
8	T003	420	871.3	0.0	10.1	5.8	415	103	3.95E+00	
8	T002	470	896.6	0.1	9.7	6.7	465	102	2.85E+00	
8	T001	510	837.1	0.0	8.6	6.1	505	101	4.11E+00	
9	T027	5	549.4	27.6	3.2	-11.7	0	128	3.38E-03	291
9	T026	36	547.2	24.8	4.3	-24.7	31	127	8.32E-03	
9	T025	61	503.7	19.6	5.7	-31.4	56	126	8.83E-03	
9	T024	86	543.2	18.8	7.3	-36.8	81	125	1.18E-02	
9	T023	111	548.0	13.0	10.2	-41.5	106	124	1.67E-02	
9	T022	151	546.9	7.9	13.1	-41.9	146	123	2.09E-02	
9	T021	191	553.2	1.2	17.1	-44.8	186	122	5.84E-01	
9	T020	231	549.8	0.6	17.2	-29.3	226	121	6.06E+00	
9	T019	271	556.0	0.1	13.0	-14.1	266	120	1.09E+01	
9	T018	311	557.1	0.0	10.5	-6.2	306	119	1.37E+01	
9	T017	351	543.7	0.0	10.0	-2.0	346	118	1.33E+01	
9	T016	391	557.9	0.0	9.4	0.8	386	117	9.94E+00	
9	T015	431	546.9	0.9	8.0	-2.3	426	116	1.08E+01	
10	T038	7	558.0	28.9	2.7	-6.7	0	139	1.79E-04	385
10	T037	40	556.4	28.6	3.0	-10.8	32	138	2.21E-03	
10	T036	85	545.2	27.7	31.8	-10.5	77	137	8.71E-04	
10	T035	135	560.8	28.2	3.6	-17.9	127	136	1.55E-03	
10	T034	185	565.3	17.5	4.2	-19.3	177	135	1.88E-03	
10	T033	235	572.1	26.6	5.2	-25.3	227	134	7.94E-03	
10	T032	280			8.9	-38.5	272	133	1.42E-02	
10	T031	310	549.9	10.1	14.2	-46.3	302	132	2.73E-02	
10	T030	335	556.6	1.1	18.9	-47.6	327	131	9.40E-01	
10	T029	365	537.1	0.3	13.8	-16.6	357	130	8.47E+00	
10	T028	405	535.2	0.0	11.7	-1.6	397	129	1.01E+01	
11	T051	8	562.1	24.3		-31.5	0	152	1.26E-02	246.0
11	T050	34	565.9	15.9	19.8	-44.1	26	151	1.19E-02	
11	T049	49	610.7	8.2	11.3	-46.1	41	150	2.31E-02	
11	T048	79	597.5	6.8	15.7	-52.4	71	149	4.94E-02	
11	T047	109	611.4	1.8	18.5	-44.9	101	148	3.89E-01	
11	T046	143.5	623.3	0.8	18.1	-42.7	136	147	5.25E+00	
11	T045	178.5	640.5	1.6	16.4	-37.6	171	146	9.78E+00	
11	T044	223.5	637.0	0.7	15.0	-24.5	216	145	1.23E+01	
11	T043	268.5	663.5	0.0	14.8	-16.3	261	144	1.32E+01	
11	T042	313.5	685.1	0.3	14.0	-10.6	306	143	1.19E+01	
11	T041	364	682.2	0.6		-9.6	356	142	9.78E+00	
11	T040	419	674.3	0.0	11.3		411	141	1.05E+01	
11	T039	471	702.9	0.2	10.2	-2.4	466	140	1.05E+01	
12	T061	5	553.2	26.6	38.5	-12.2	0	162	9.50E-04	317.0
12	T060	30	581.2	28.2	3.4	-15.3	25	161	1.22E-03	
12	T059	55	558.1	27.4	3.3	-14.3	50	160	9.88E-04	
12	T058	80	560.1	27.4	3.6	-17.1	75	159	1.07E-03	
12	T056	150	563.8	25.6	4.9	-23.4	145	157	1.50E-03	
12	T057	155.5			4.0	-19.1	110	158	2.37E-03	

12	T055	185	565.2	23.9	5.8	-27.2	180	156	3.19E-03	
12	T054	220	561.9	19.7	8.1	-33.5	215	155	6.22E-03	
12	T053	255	567.0	15.1	10.7	-38.5	250	154	1.05E-02	
12	T052	295	563.1	2.9	16.1	-39.8	290	153	6.86E-01	
13	T071	5	558.0	27.3	4.4	-15.0	0	172	1.23E-03	260.0
13	T070	47	541.8	24.0	7.4	-25.4	42	171	6.15E-03	
13	T069	82	562.4	19.3	9.4	-39.2	77	170	1.00E-02	
13	T068	122	575.7	15.7	13.1	-43.7	117	169	1.44E-02	
13	T067	162	578.2	10.3	13.1	-47.0	157	168	2.13E-02	
13	T066	202	585.0	5.1	13.4	-43.9	197	167	3.96E-02	
13	T065	242	588.8	0.9	19.7	-46.2	237	166	6.94E-01	
13	T064	277	631.3	0.0	18.4	-40.5	272	165	5.95E+00	
13	T063	307	593.1	0.6	15.9	-27.5	302	164	1.27E+01	
13	T062	342	616.9	0.6	11.5	-11.2	337	163	1.56E+01	
14	T084	5	551.7	8.6	14.4	-42.6	0	185	4.20E-04	504.0
14	T083	50	567.9	29.1	32.8	-6.4	45	184	1.81E-03	
14	T082	100	560.5	27.0	3.7	-15.9	95	183	1.89E-03	
14	T081	160	562.9	26.7	4.4	-18.6	155	182	2.03E-03	
14	T080	210	557.1	26.9	4.2	-18.7	205	181	3.07E-03	
14	T079	265	561.5	25.9	55.4	-21.4	260	180	3.54E-03	
14	T078	315	553.6	24.0	5.6	-26.1	310	179	3.24E-03	
14	T077	355	568.4	23.7		-28.0	350	178	4.61E-03	
14	T076	395	561.3	22.8	7.3	-28.6	390	176	3.71E-02	
14	T075	430	551.3	22.2	7.3	-30.9	425	175	4.47E-03	
14	T074	458	560.5	27.4	9.7	-35.7	453	177	1.06E-02	
14	T073	480	554.8	1.4	18.6	-43.6	475	174	3.69E-01	
14	T072	520	551.2	0.6		-24.8	515	173	8.63E+00	
15	T092	5	554.5	28.6	2.5	-7.2	0	193	2.44E-04	215.0
15	T091	75	559.6	26.1	4.0	-17.3	70	192	2.82E-03	
15	T090	115	555.4	24.9	4.4	-18.5	110	191	3.81E-03	
15	T089	155	562.6	22.6	5.5	-23.9	150	190	4.74E-03	
15	T088	195	558.7	16.0	30.1	-28.4	190	189	2.79E-03	
15	T087	235	556.3	0.0	10.1	-32.2	230	188	1.32E-03	
15	T086	285	564.6	0.4	14.2	-34.3	280	187	1.72E-01	
15	T085	325	563.7	0.6	10.0	-22.0	320	186	2.85E+00	